Journal of Membrane Science 494 (2015) 8–24

Contents lists available at ScienceDirect

Journal of Membrane Science

journal homepage: www.elsevier.com/locate/memsci

# Performance of spiral-wound membrane modules in organic solvent nanofiltration – Fluid dynamics and mass transfer characteristics

Binchu Shi [a,b], Patrizia Marchetti [b], Dimitar Peshev [c], Shengfu Zhang [a], Andrew G. Livingston [a,b,*]

[a] Evonik Membrane Extraction Technology Limited, Unit 6 Greenford Park, Ockham Drive, Greenford, London UB6 0AZ, United Kingdom
[b] Department of Chemical Engineering, Imperial College London, Exhibition Road, London SW7 2AZ, United Kingdom
[c] Department of Chemical Engineering, University of Chemical Technology and Metallurgy, 8, Kl. Ohridsky Blvd, Sofia 1756, Bulgaria

ARTICLE INFO

*Article history:*
Received 8 April 2015
Received in revised form
6 July 2015
Accepted 20 July 2015
Available online 21 July 2015

*Keywords:*
Spiral-wound membrane module
Organic solvent nanofiltration
Pressure drop
Mass transfer coefficient

ABSTRACT

During the past few decades organic solvent nanofiltration has received a great deal of attention and a growing number of studies has been reported on development and optimisation of solvent resistant membranes and their transport mechanism. However, most of these studies have used flat sheet membranes. On the other hand, many researchers studied fluid dynamics and mass transfer in spiral-wound membrane modules, almost exclusively in aqueous solutions. This paper reports the performance of four spiral-wound membrane modules tested in 0–20 wt% solutions of sucrose octaacetate in ethyl acetate under various pressures and retentate flowrates. These modules were made of two different types of membranes (a commercial membrane, PuraMem® S600, and a development product, Lab-1, from Evonik Membrane Extraction Technology Limited) and covered three module sizes (1.8″ × 12″, 2.5″ × 40″ and 4.0″ × 40″). All modules had the same feed and permeate spacers. The classical solution diffusion model was applied to describe the transport of solute and solvent through the membrane and regress the unknown model parameters from flat sheet data. Correlations for characterising the fluid dynamics and mass transfer in the spiral-wound membrane modules, as well as the parameters describing the feed and permeate channels, were determined by performing the regression of experimental data of a 1.8″ × 12″ PuraMem® S600 membrane module. The classical solution–diffusion model, combined with the film theory, was then successfully applied to predict the performance of other modules of larger size (such as the 2.5″ × 40″ and 4.0″ × 40″ module sizes) and/or made of a different membrane material (such as Lab-1). The procedure proposed in this paper predicts the performance of a specific module by obtaining a limited number of experimental data for flat sheets and a 1.8″ × 12″ spiral-wound membrane module only (necessary to obtain the fitting parameters characteristic of the membrane and the module). Furthermore, with this procedure, it is not necessary to know a priori the spacer geometry, because the necessary information about the spacer geometry will be also obtained by regression of few experimental data.

© 2015 Published by Elsevier B.V.

## 1. Introduction

During the past few decades, organic solvent nanofiltration (OSN) has received a great deal of attention in industry, with applications ranging from solute enrichment and solvent recovery to impurity removal and catalyst recycle [1–4]. The development of a membrane process, such as OSN, usually involves several stages, starting from feasibility tests at laboratory scale, passing through pilot plant tests and finishing with large industrial scale processes, and the availability of a reliable simulation model could make the transition between these stages smoother and easier. Three levels can be distinguished within the general process modelling framework: membrane transport at molecular level, fluid dynamics and mass transfer in membrane modules and performance at process level [5]. Many studies on the transport mechanism through OSN membranes have been published; however, most of these studies were made using flat sheet membranes and at the level of molecular transport. Only few studies [1,6,7] described the performance of OSN processes with spiral-wound membrane modules using some simple, non-predictive membrane transport models; however, the effects of the modules at process level were

*Abbreviations:* CFD, computational fluid dynamics; EA, ethyl acetate; OSN, organic solvent nanofiltration; SoA, sucrose octaacetate; UNIF-DMD, Dortmund modified UNIFAC method

* Corresponding author at: Department of Chemical Engineering, Imperial College London, Exhibition Road, London, SW7 2AZ, United Kingdom.
*E-mail address:* a.livingston@imperial.ac.uk (A.G. Livingston).

http://dx.doi.org/10.1016/j.memsci.2015.07.044
0376-7388/© 2015 Published by Elsevier B.V.

not explored. To the best of the authors' knowledge, in the literature, there has been only one study which investigated fluid dynamics and mass transfer characteristics in a spiral-wound membrane module for OSN. In that study, Silva et al. [8] reported the experimental and simulated performance of a 2.5″ × 40″ spiral-wound STARMEM™ 122 membrane module in 0–20 wt% solutions of tetraoctylammonium bromide in toluene using a steady-state approach. In their modelling, two solution–diffusion based models were used and the corresponding model parameters were determined from flat sheet data; the former approach was a simple model, which assumed uniform pressure and concentration in both feed and permeate sides, while the latter was a complex model, which considered spatial concentration, velocity and pressure gradients. Although both models showed good agreement with the experimental data for the system under study, the authors pointed out that the complex model is more appropriate when the assumptions of both pressure and mass transfer coefficient constancy are not acceptable. The pressure drop and mass transfer correlations used in their study were adapted from Schock and Miquel's work [9]. Finally, in their study, the effects of membrane type and module size on the overall process performance were not explored.

Although the literature on spiral-wound membrane modules in OSN is scarce, many researchers studied fluid dynamics and mass transfer through plane, spacer-filled channels, characteristics of spiral-wound membrane modules, in aqueous solutions. To determine the mass transfer coefficient, three main methods have been used in the literature [9–24]: (i) direct measurements, which made use of optical or electrochemical methods; (ii) indirect measurements, which were based on regression of membrane performance data using a combination of film theory and membrane transport models; and (iii) computational fluid dynamics (CFD) simulations, which were based on a priori simulation of the module geometry. The pressure drop characteristics of a module were usually determined either from direct measurements, using accurate pressure gauges, or via CFD simulations [9,12–16,23].

Among the direct measurement studies, Johnson [10] applied an interferometer with a helium-neon laser as a light source to measure concentration polarisation in a reverse osmosis system. However, this method introduced a significant error due to the deflection of the light from a solute even in dilute conditions. Balster et al. [11] studied the effects of various single and multi-layer spacers on mass transfer using the limiting current technique. They concluded that the multi-layer spacer configurations exhibited significant mass transfer enhancement with respect to single-layer ones. However, in their work, the flow was passed along impermeable channel walls, which are obviously different from the semi-permeable membrane walls, presenting in a membrane module. Schock and Miquel [9] measured the pressure drop through various feed and permeate spacer filled channels. A friction coefficient correlation was used to fit their experimental data, in the form of Eq. (1):

$$f = \frac{2\Delta P d_h}{\rho u^2 L} = a\left(\frac{d_h \rho u}{\mu}\right)^b = aRe^b \tag{1}$$

$f$ is the friction coefficient and $\Delta P$ is the pressure drop through the channel. $d_h$ is the hydraulic diameter of the channel, $L$ is the length of the channel, $\rho$ is the density of the solution, $u$ is the velocity of the flow along the channel, $\mu$ is the dynamic viscosity of the solution and $Re$ is the Reynolds number. $a$ and $b$ are the coefficient and the exponent of Reynolds number in the friction coefficient correlation, respectively. In Schock and Miquel's work, the spacer geometry was measured using a light microscope; however the authors pointed out that this might not be a very accurate technique to obtain the characteristic dimensions of permeate spacers, due to their complicated geometry. They found that the geometry of the feed spacer had little effect on the friction coefficient, while the geometry of the permeate spacer showed more significant effects. Kuroda et al. [12], Da Costa et al. [13] and Schwinge et al. [14] also studied the effects of spacer geometry on the friction coefficient. Various types of spacers were considered in their work and a number of experimentally measured pressure drop data were reported. The significant effects of the spacer geometry on pressure drop performance were observed.

Among the indirect measurement approaches, Schock and Miquel [9] performed regression of flat sheet membrane performance data to determine the mass transfer coefficient in a plane, feed spacer filled channel using the combination of film theory and an empirical membrane transport model. This empirical transport model assumes that the permeate flux is linearly dependant on the difference between applied pressure and osmotic pressure. The authors used a dimensionless correlation to describe the mass transfer coefficient, in the form of Eq. (2):

$$Sh = \frac{kd_h}{D} = \alpha Re^{\beta} Sc^{\lambda} = \alpha\left(\frac{d_h \rho u}{\mu}\right)^{\beta}\left(\frac{\mu}{\rho D}\right)^{\lambda} \tag{2}$$

$Sh$ and $Sc$ are the dimensionless Sherwood and Schmidt numbers, respectively. $\alpha$, $\beta$ and $\lambda$ are the coefficient and the exponents in the Sherwood correlation equation. $k$ is the mass transfer coefficient and $D$ is the diffusivity of a solute in a solvent. Four types of commercial feed spacers were studied in their work; interestingly, no effect of the spacer geometry on the mass transfer coefficient was observed. A similar methodology was used by Da Costa et al. [13] and Schwinge et al. [14], who on the other hand, found that the spacer geometry does affect the mass transfer coefficient in spiral-wound membrane modules. Interestingly, their correlations [13,14] for the same spacers showed good agreement. Although the simple, empirical membrane transport model worked well in these studies carried out in dilute aqueous solutions [9,13,14], it has yet to be established whether the model will describe mass transfer during OSN in spiral-wound membrane modules.

Finally, among the CFD studies on the mass transfer coefficient, Da Costa et al. [15] and Karode and Kumar [16] performed 2 dimensional CFD simulations to visualize the fluid flow structure through various spacer filled flat channels. They found that the flow path was affected by a combination of flow attack angle, filament size, mesh size and angle between crossing filaments. Their friction coefficient correlations for the same spacers showed good agreement. Li et al. [17–19] performed 3 dimensional CFD simulations to study flow characteristics and mass transfer in spacer-filled channels and the results were compared with their experimental data. Good agreement was reported and various correlations in the form of Eq. (2) were presented. Fimbre-Weihs and Wiley [20] presented both 2 and 3 dimensional CFD simulations to study mass transfer in a spacer filled channel, positioned at 45° and 90°, with a single Schmidt number ($Sc = 600$). The authors reported that the exponent of Reynolds number in the Sherwood correlation, represented in the form of Eq. (2), is 0.591. Koutsou et al. [21] even reported a significant amount of mass transfer coefficient data for ten types of spacers and discussed the effect of Schmidt number on the mass transfer coefficient using CFD simulations. Furthermore, various Sherwood correlations were reported based on average mass transfer coefficients and good agreement with Li et al.'s work [19] was observed. Kostoglou and Karabelas [22] developed a comprehensive model which incorporates small scale CFD results on the retentate side and accounts for permeate variables as a step forward to predict the performance of spiral-wound membrane modules in desalination. Karabelas et al. [23] performed a parametric study on the

performance of spiral-wound membrane modules in steady state mode in desalination using an advanced simulator, considering pressure drops and mass transfer characteristics obtained from CFD, and reported on the importance of spacer geometry and membrane envelope width on module performance. CFD studies supply understanding and visualisation of the flow path and the mass transfer in spacer-filled channels and give knowledge on the optimisation of spacer geometry. However, most of these studies were made using simple-geometry spacers with regular filament shapes such as ladder spacers with cylindrical filaments. In commercial modules, many spacers with much more complex geometry are used, such as cylindrical filaments with some cut-offs and with woven multi-layer structure. Besides, information about the spacer geometry in commercial modules is usually confidential and therefore unavailable for users without performing a module autopsy. All these factors make CFD simulations more complicated to use.

From all the literature so far, it is clear that the spacer geometry significantly affects the fluid dynamics and mass transfer characteristics in the spacer filled channels of spiral-wound membrane modules. Accordingly, many correlations in the form of Eqs. (1) and (2) were reported. However, all these correlations were derived in aqueous solutions and no work so far has numerically related the spacer geometry with the values of the coefficients and the exponents in the friction coefficient and Sherwood number correlations. In comparison to desalination, the variety of solvents and solutes in OSN makes fluid dynamics and mass transfer characteristics in spiral-wound membrane modules even more complicated due to a broad range of possible Reynolds and Schmidt numbers. Considering that the collection of experimental data for all the possible modules and solute/solvent combinations would be prohibitively time consuming, it is useful to have a simple procedure to predict the permeation flux and rejection of different modules, based on the knowledge of the transport through the flat sheet membrane and the fluid dynamics and mass transfer characteristics of a small module. From a design and prediction point of view, there are still challenges to select/generate suitable correlations for describing the fluid dynamics and mass transfer characteristics in spiral-wound membrane modules for OSN applications.

In this work, the performance of four spiral-wound membrane modules tested in 0–20 wt% solutions of sucrose octaacetate (SoA) in ethyl acetate (EA) under various pressures and retentate flowrates is presented and discussed. These modules were made of two different types of membranes (a commercial membrane, PuraMem® S600, and a development product, Lab-1, from Evonik Membrane Extraction Technology Limited (Evonik MET)) and covered three module sizes (1.8″ × 12″, 2.5″ × 40″ and 4.0″ × 40″). All modules had the same feed and permeate spacers (referred to as EMET-F3 and EMET-P1, respectively). The classical solution diffusion model was applied to describe the transport of solute and solvent through the membrane and regress the unknown model parameters from flat sheet performance data. Correlations for characterising the fluid dynamics and mass transfer in the spiral-wound membrane modules, as well as the parameters describing the geometry of both the feed and permeate channels, were determined by regression of experimental data of a 1.8″ × 12″ PuraMem® S600 membrane module. The classical solution-diffusion model, combined with the film theory, was then successfully applied to predict the performance of other three modules of larger size (such as the 2.5″ × 40″ and 4.0″ × 40″ module sizes) and/or made of a different membrane material (such as Lab-1). In conclusion, the procedure proposed in this paper predicts the performance of a specific module by obtaining a limited number of experimental data for flat sheets and a 1.8″ × 12″ spiral-wound membrane module only (necessary to obtain the fitting parameters characteristic of the membrane and the module). Furthermore, with this procedure, it is not necessary to know a priori the spacer geometry, because the necessary information about the spacer geometry will be also obtained by regression of few experimental data.

## 2. Materials and methods

### 2.1. Materials

Analytical grade EA was purchased from Tennants Distribution Limited, UK. SoA (> 97% purity) was purchased from Sigma Aldrich Limited, UK. EA was chosen as a solvent because it is commonly used in industry. SoA was chosen as a solute, for its good solubility in EA and its low price, which are important factors when carrying out experiments at a large scale and using highly concentrated solutions, such as in this study.

Flat sheets of PuraMem® S600 (PM S600, A4 size) were provided by Evonik MET. Evonik MET also provided flat sheets of a development rubbery membrane, referred to as Lab-1 in this study. According to Evonik MET's specifications, Lab-1 is tighter than PM S600. As shown in Fig. 1, the thickness of the top silicon layer of the Lab-1 membrane is about 100 nm.

Four spiral-wound membrane modules were also provided by Evonik MET, three of them made of PM S600 membrane and the other one made of Lab-1 membrane. All modules had the same feed and permeate spacers (referred to as EMET-F3 and EMET-P1, respectively). Both the length and width of the permeate channel ($L_P$ and $W_P$, respectively) are about 70 mm shorter than the feed channel due to the presence of glue lines on the permeate side. The details about the configuration of these four modules are summarised in Table 1.

### 2.2. Methods

#### 2.2.1. Performance of flat sheet membranes

Solvent flux and solute rejection of both flat sheet PM S600 and Lab-1 membranes were measured in a 4-cell cross-flow filtration system, as shown in Fig. 2(a). The flat sheet membranes were initially conditioned at 5 bar for 5–7 h using pure EA to remove the preservatives inside the membranes. The membranes were then tested in pure EA, followed by 1 g $L^{-1}$ SoA in EA solution at various feed pressures (from 5 to 30 bar in increasing order 5 → 10 → 20 → 30, and then in decreasing order back to 5 bar) with a retentate flowrate of 80 L $h^{-1}$ (obtained with a Hydra-Cell D3 pump). The volume of the feed solution was around 3.5 L. This pressurisation and depressurisation test was repeated three times for each membrane. Four discs of the same membranes were tested simultaneously in the cross-flow equipment. In total, two test runs were performed for each type of membrane. The permeate flux was measured every hour until the flux had remained stable for 3 h under each test condition. The average of the last three

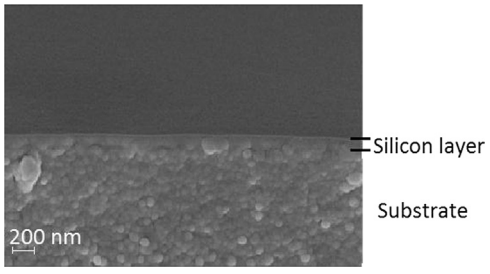



**Fig. 1.** Scanning electron microscope image of the cross section of Lab-1 membrane.

**Table 1**
Configuration of the four spiral-wound membrane modules (SWMM) used in this study. All information is provided by the supplier.

| Module code | Module size | Membrane type | Membrane area ($m^2$) | Number of leaves | Module body length (mm) |
|---|---|---|---|---|---|
| SWMM-1 | 1.8″ × 12″ | PM S600 | 0.14 | 1 | 175 |
| SWMM-2 | 2.5″ × 40″ | PM S600 | 1.74 | 2 | 886 |
| SWMM-3 | 4.0″ × 40″ | PM S600 | 5.19 | 4 | 886 |
| SWMM-4 | 2.5″ × 40″ | Lab-1 | 1.87 | 2 | 886 |

measurements was recorded as the membrane flux. Permeate and retentate samples were taken at 3 different time points with one hour interval after the steady-state flux condition was reached. The average of these three rejections was recorded as the membrane rejection.

*2.2.2. Performance of spiral-wound membrane module*

All the spiral-wound membrane modules were initially conditioned at 5 bar for 5–7 h using pure EA to remove the preservatives from the membrane. These modules were then tested in pure EA at 30 °C and various feed pressures (from 10 to 30 bar in increasing order: 10 → 20 → 30). After that, the modules were tested in solutions of SoA in EA with different concentrations

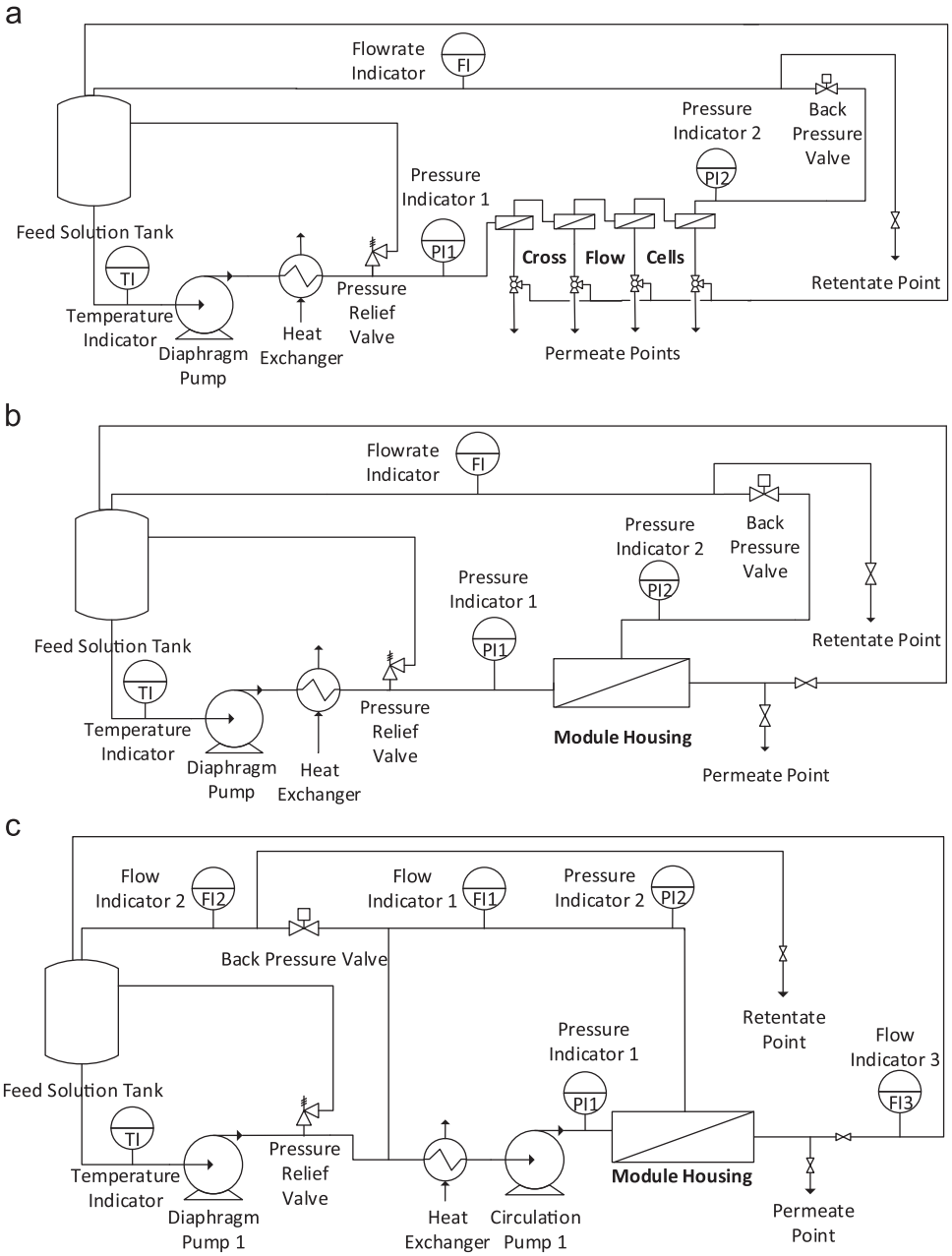



**Fig. 2.** Schematic diagrams of the module testing equipment: (a) single-pump configuration for the flat sheet membrane test; (b) single-pump configuration for the smallest SWWM-1 module test (1.8″ × 12″) and the intermediate SWWM-2 and SWWM-4 module tests (2.5″ × 40″); (c) two-pump configuration for the largest SWWM-3 module test (4.0″ × 40″).

**Table 2**
Structure of sucrose octaacetate by means of UNIF-DMD structural groups.

| Group code | Group | Number of appearance |
|---|---|---|
| 1505 | $CH_3COO$ | 8 |
| 1605 | CHO | 3 |
| 1030 | c-CH | 5 |
| 1025 | c-C | 1 |
| 1010 | $CH_2$ | 3 |

(from low concentration to high concentration in increasing order: 1 wt% → 10 wt% → 20 wt%). In each solution, the modules were tested at various feed pressures (10, 20 and 30 bar) with 3 or 4 different retentate flowrates. The permeate flux was measured every hour until the flux had remained stable for 3 h under each test condition. The average of the last three measurements was recorded as the module flux. Permeate and retentate samples were taken at 3 different time points with one hour interval after the steady-state flux condition was reached. The average of these three rejections was recorded as the module rejection. To allow for suitable flowrates in each module size, different test equipment was used for the different modules. The smallest SWMM-1 module (1.8″ × 12″) and the intermediate SWMM-2 and SWMM-4 modules (2.5″ × 40″) were tested in a system provided with a single diaphragm pump, as shown in Fig. 2(b), whereas the largest SWMM-3 module (4.0″ × 40″) was tested in a two-pump system, as schematically shown in Fig. 2(c). Specifically, the smallest SWMM-1 module was tested using the same diaphragm pump as in the flat sheet membrane test equipment (Hydra-Cell D3), where the flowrate was varied from 80 to 240 L $h^{-1}$. Differently, the SWMM-2 and SWMM-4 modules were tested using a more powerful diaphragm pump, capable of controlling the flowrate from 200 to 1000 L $h^{-1}$ (Hydra-Cell D10). Finally, to test the largest SWMM-3 module, a circulation pump was used to provide the flowrate through the module, up to 3000 L $h^{-1}$ (Peripheral-Pump HMH125), while a separate diaphragm pump was used to feed the recirculating solution into the retentate loop (Hydra-Cell D3) (see Fig. 2(c)). The fluid flowrate after the back pressure valve was controlled to be around 75 L $h^{-1}$, 155 L $h^{-1}$ and 230 L $h^{-1}$ at the feed pressure of 10 bar, 20 bar and 30 bar, respectively. The volume of the feed solution in the tests for the 1.8″, 2.5″ and 4.0″ modules was around 3.5 L, 30 L and 40 L, respectively. For all the module sizes, the pressure drop through the empty housing was measured before the installation of the module.

#### 2.2.3. Analytical methods

Solute rejection ($Rej_i^{obs}$) and permeate flux ($J_V$) were calculated as reported in Eqs. (3) and (4), respectively.

$$Rej_i^{obs} = \left(1 - \frac{C_{i,P}}{C_{i,R}}\right)\cdot 100\% \tag{3}$$

$$J_V = \frac{V}{t\cdot A} \tag{4}$$

$C_{i,R}$ and $C_{i,P}$ are the concentrations at retentate side and permeate side, respectively. $V$ is the total permeate volume collected during the permeation time $t$, and $A$ is the effective membrane area. The concentration of SoA was determined using a gas chromatograph with a flame ionisation detector and a fused silica column (Rtx® – 2887 column purchased from Thames Restek Limited, UK). The temperature programme ran from 40 to 300 °C at a rate of 15 °C $min^{-1}$, and then remained at 300 °C for 10 min. The flow rate of the carrier gas (helium) was set at 0.7 ml $min^{-1}$.

## 3. Modelling and analysis

### 3.1. Physical properties of solutions

In this work, the properties of SoA/EA solutions were determined using the Aspen Properties Estimate System. Dortmund modified UNIFAC (UNIF-DMD) method was applied as a base method. EA was selected from Aspen Properties database. As the UNIF-DMD parameters for SoA are not available in Aspen, the structure of SoA was defined by means of UNIF-DMD structural groups (see Table 2) and molecular weight (678.59 g $mol^{-1}$). NISTs Thermodynamic Engine was used to estimate all needed parameters for the two species.

The calculated dynamic viscosity ($\mu_F$), density ($\rho_F$), activity coefficient of SoA ($\gamma_{F,1}$), activity coefficient of EA ($\gamma_{F,2}$) and diffusivity of SoA in EA ($D_F$), in the solutions with different concentrations of SoA at 30 °C, were correlated with second order polynomials. These correlations are shown as Eqs. (5–9).

$$\mu_F = \left(18.3w_{F,1}^2 + 4.3w_{F,1} + 4.1\right)\times 10^{-4} \tag{5}$$

$$\rho_F = 330.1w_{F,1}^2 + 70.1w_{F,1} + 892.7 \tag{6}$$

$$\gamma_{F,1} = 12.1w_{F,1}^2 - 8.91w_{F,1} + 2.77 \tag{7}$$

$$\gamma_{F,2} = 0.213w_{F,1}^2 + 0.0026w_{F,1} + 1 \tag{8}$$

$$D_F = \left(-6.59w_{F,1}^2 - 28.6w_{F,1} + 23.8\right)\times 10^{-10} \tag{9}$$

$w_{F,1}$ is the mass fraction of SoA in the solution. The $R^2$ values of all these correlations are larger than 0.9995.

### 3.2. Procedure for regression and prediction

To study the fluid dynamics and mass transfer characteristics of the spiral-wound membrane modules, the following procedure, was performed:

(a) a suitable membrane transport model was chosen to describe the transport through the membrane and experimental data for flat sheet membranes were used to perform regression and obtain the unknown model parameters;
(b) experimental data for a 1.8″ × 12″ spiral-wound membrane module were used to perform regression and obtain semi-empirical correlations for the pressure drop in both the feed and permeate channels and the mass transfer coefficient in the feed channel; the parameters describing the feed and permeate channels in the spiral-wound membrane module were also obtained in this regression step;
(c) experimental data for larger spiral-wound membrane modules, fabricated using the same feed and permeate spacers, were used to validate the predictive capability of this procedure.

The procedure is schematically illustrated in Fig. 3.

#### 3.2.1. Membrane transport model and regression of the permeability coefficients

In the literature, different studies have been reported on the characterisation of the transport mechanism through nanofiltration membranes. Marchetti and Livingston [25] reported a systematic comparison of the different membrane transport models using selected experimental data for various solvents and solutes through four commercial OSN membranes (DuraMem® 200,

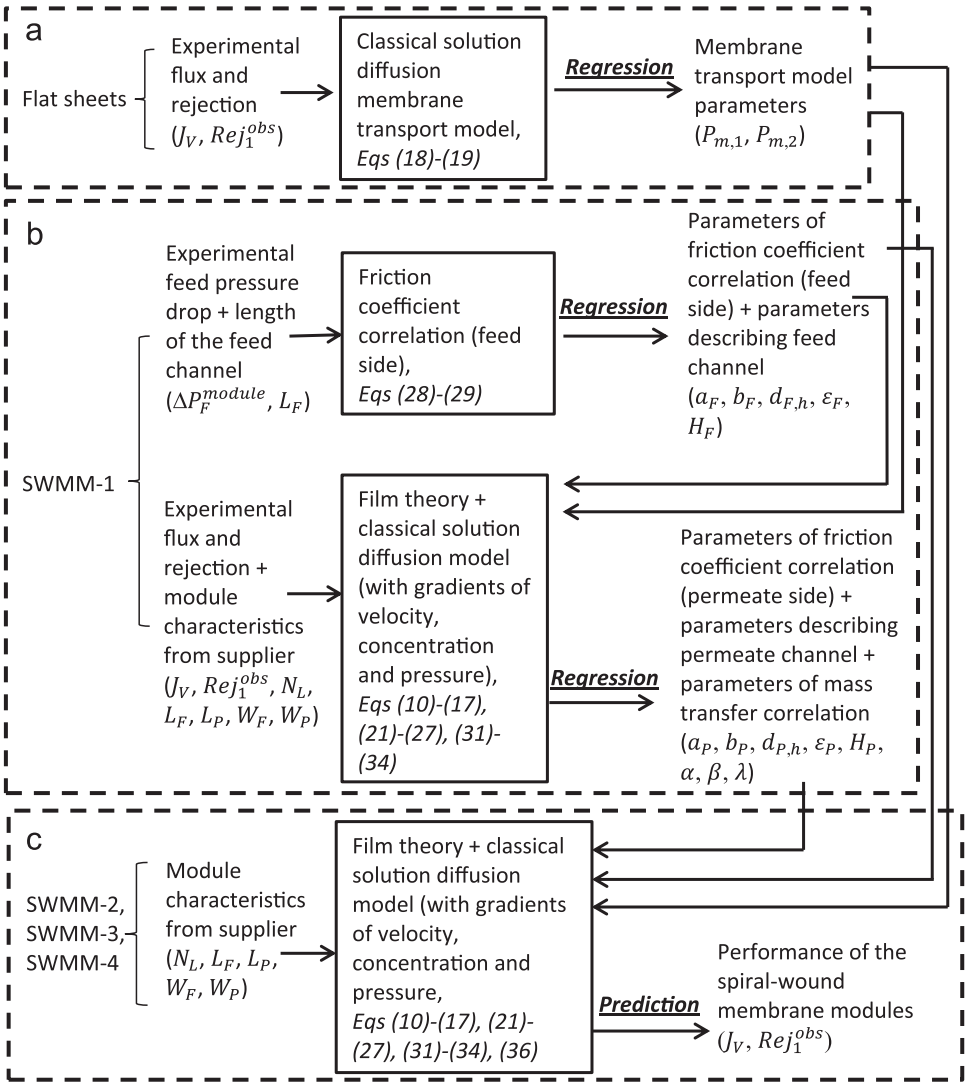



**Fig. 3.** Schematic diagram of the procedure for regression and prediction used in this work. (a) Regression of the flat sheet experimental data to obtain the membrane transport model parameters; (b) regression of a 1.8″ × 12″ module (SWMM-1) performance data to obtain semi-empirical expressions for the pressure drop in both the feed and permeate channels and the mass transfer coefficient in the feed channel, as well as the parameters describing the feed and permeate channels; (c) prediction of performance for spiral-wound membrane modules of different sizes, but with the same feed and permeate spacers.

DuraMem® 500, PuraMem® 280 and PuraMem® S600). They concluded that solution–diffusion based models give a better description of permeation through flexible chain glassy membranes and rubbery membranes than pore flow based models. Similarly, Silva et al. [8], Han et al. [26] and Peeva et al. [27] studied the permeation of pure organic solvents and organic solvent/water mixtures through STARMEM™ 122 membranes and concluded that the solution diffusion model gives a better prediction than the pore flow model. In order to describe membrane transport in the presence of highly concentrated solutions, Silva et al. [8] and Peeva et al. [27] considered the thermodynamic non-ideality of the solution and the occurrence of concentration polarisation, by introducing activity coefficients and the film theory into the classical solution diffusion model. This is described by Eqs. (10–17) for a two-component system (one solute and one solvent).

$$J_1 = P_{m,1}\left[x_{1,FM} - x_{1,P}\frac{\gamma_{1,P}}{\gamma_{1,FM}}\exp\left(-\frac{\nu_1(P_F - P_P)}{RT}\right)\right] \quad (10)$$

$$J_2 = P_{m,2}\left[x_{2,FM} - x_{2,P}\frac{\gamma_{2,P}}{\gamma_{2,FM}}\exp\left(-\frac{\nu_2(P_F - P_P)}{RT}\right)\right] \quad (11)$$

$$J_V = J_1\nu_1 + J_2\nu_2 \quad (12)$$

$$\frac{C_{1,FM} - C_{1,P}}{C_{1,F} - C_{1,P}} = \exp\left(\frac{J_V}{k_F}\right) \quad (13)$$

$$x_{1,FM} + x_{2,FM} = 1 \quad (14)$$

$$x_{1,P} + x_{2,P} = 1 \quad (15)$$

$$x_{1,FM} = \frac{C_{1,FM}}{C_{1,FM} + C_{2,FM}} \quad (16)$$

$$x_{1,P} = \frac{C_{1,P}}{C_{1,P} + C_{2,P}} \quad (17)$$

$P_{m,i}$ is the permeability coefficient for the species $i$ ($i = 1$,

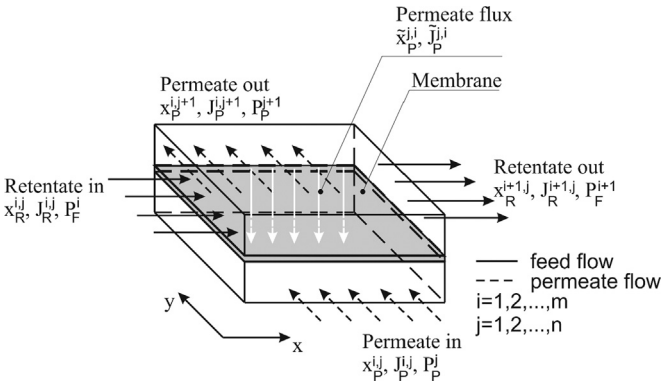



**Fig. 4.** Schematic representation of an elemental volume of a spiral-wound membrane module, containing parts of the feed channel, the membrane layer and the permeate channel. Within each elemental volume, constant local pressure, concentration and velocity values were assumed.

solute; $i = 2$, solvent). $k_F$ is the mass transfer coefficient in the feed side. $J$ is the molar flux, $x$ is the molar fraction, $\gamma$ is the activity coefficient, $\nu$ is the molar volume, $P$ is the pressure, $R$ is the ideal gas constant, $T$ is the temperature, $C$ is the concentration and $J_V$ is the total volumetric flux. The subscripts $P$, $F$ and $FM$ refer to the permeate side, the feed side and the feed side membrane–liquid interface, respective. The membranes used in this study consist of a rubbery separation layer cast on an ultrafiltration support, and belong therefore to the class of membranes characterised by a solution–diffusion transport mechanism, according to Marchetti and Livingston [25]. In order to account for mass transfer limitations and thermodynamic non-ideality of the solutions, Eqs. (10–17) were used in this work, where species 1 is SoA and species 2 is EA.

The permeability coefficients of the classical solution–diffusion model for SoA and EA ($P_{m,1}$ and $P_{m,2}$, respectively) were determined by performing regression of the flat sheet flux and rejection data obtained at the lowest practical operating pressure of 5 bar with a retentate flowrate of 80 L h$^{-1}$ (see Fig. 4(a)). To perform this regression, the following assumptions were made [27]: (i) negligible pressure drops through feed and permeate sides; (ii) negligible concentration polarisation; (iii) thermodynamically ideality of the system. Therefore, the classical solution diffusion model (Eqs. (10) and (11)) was simplified as the follows:

$$J_1 = P_{m,1}\left[x_{1,F} - x_{1,P}\exp\left(-\frac{\nu_1 P_F}{RT}\right)\right] \tag{18}$$

$$J_2 = P_{m,2}\left[x_{2,F} - x_{2,P}\exp\left(-\frac{\nu_2 P_F}{RT}\right)\right] \tag{19}$$

The calculated permeability coefficients were used to predict the performance of the flat sheet membranes tested at different operating pressures, to further verify the suitability of this membrane transport model for the membranes used in this study. The capability of the model to perform regression was quantified in terms of norm of residuals, *resnorm*, as shown in Eq. (20).

$$resnorm = \left(\frac{1}{Q-1}\sum_{q=1}^{Q}\left(\frac{z_{q,c} - \bar{z}_{q,e}}{\bar{z}_{q,e}}\right)^2\right)^{0.5} \tag{20}$$

In this equation, $z_{q,c}$, $\bar{z}_{q,e}$ and $Q$ are the calculated data, average experimental data, and the number of the data, respectively.

### 3.2.2. Pressure drops and mass transfer characteristics in spiral-wound membrane modules

Permeate and feed channels in spiral-wound membrane modules were modelled as composed of $m \times n$ sufficiently small volumes in 2 dimensions, within which constant local pressure, concentration and velocity values were assumed. This is schematically shown in Fig. 4.

The permeate molar flowrate, $\tilde{J}_P^{i,j}$, and the solute molar fraction, $\tilde{x}_P^{i,j}$, through each $i \times j$ membrane element was calculated as a function of the local feed and permeate pressures and concentrations, using the solution diffusion model, as described by Eqs. (10–17). As constant local pressures, velocity and concentrations were considered within each element, the flux and solute molar fraction through the element were calculated using the values of the parameters at the inlet of the element. One-dimensional convective flow was assumed along the $x$ axis in the feed channel and along the $y$ axis in the permeate channel. The concentration profiles along $x$ and $y$ directions were obtained as a result of consecutive solutions of the coupled membrane transport model (see Eqs. (10–17)) and the material balance equations (see Eqs. (21–24)) for each pair of $i \times j$ permeate and feed elemental volume.

$$J_P^{i,j+1} = J_P^{i,j} + \tilde{J}_P^{i,j} \tag{21}$$

$$x_P^{i,j+1} J_P^{i,j+1} = x_P^{i,j} J_P^{i,j} + \tilde{x}_P^{i,j} \tilde{J}_P^{i,j} \tag{22}$$

$$J_R^{i+1,j} = J_R^{i,j} - \tilde{J}_P^{i,j} \tag{23}$$

$$x_R^{i+1,j} J_R^{i+1,j} = x_R^{i,j} J_R^{i,j} - \tilde{x}_P^{i,j} \tilde{J}_P^{i,j} \tag{24}$$

$J_R$ and $J_P$ are the molar flowrate of the retentate and permeate flow, respectively. $x_R^{i,j}$ is the local solute molar fraction in the retentate side and $x_P^{i,j}$ is the local solute molar fraction in the permeate side. The pressure drop through the feed channel was calculated using the friction coefficient correlation in the form of Eq. (1). This equation was reformulated to describe the pressure drop along the elemental volume, as shown in Eq. (25).

$$P_F^{i+1} = P_F^i - \frac{a_F}{2d_{F,h}}\left(\frac{\rho_{\left(\bar{x}_R^i\right)}\bar{u}_{i,F} d_{F,h}}{\mu_{\left(\bar{x}_R^i\right)}}\right)^{b_F} \rho_{\left(\bar{x}_R^i\right)}\bar{u}_{i,F}^2 \Delta x^i \tag{25}$$

$a_F$ and $b_F$ are the coefficient and the exponent of the Reynolds number in the friction coefficient correlation for the feed channel, respectively. $d_{F,h}$ is the hydraulic diameter of the feed channel and $\Delta x^i$ is the length of the element $i \times j$ along $x$ axis. In Eq. (25), the average retentate mole fraction, $\bar{x}_R^i$, and the average linear fluid velocity, $\bar{u}_{i,F}$, for the entire cross section of the feed channel, at axial position $x^i$, were calculated according to Eqs. (26) and (27), respectively.

$$\bar{x}_R^i = \frac{\sum_{j=1}^{n} x_R^{i,j} J_R^{i,j}}{\sum_{j=1}^{n} J_R^{i,j}} \tag{26}$$

$$\bar{u}_{i,F} = \frac{\sum_{j=1}^{n} J_R^{i,j} \nu_{\left(\bar{x}_R^i\right)}}{N_L \times H_F L_F \varepsilon_F} \tag{27}$$

$\varepsilon_F$ is the void fraction of the feed spacer, $H_F$ is the height of the feed spacer, $N_L$ is the number of the membrane leaves, $L_F$ is the length of the feed channel. The unknown parameters describing the coefficient and the exponent of the Reynolds number in the friction coefficient correlation for the feed channel ($a_F$ and $b_F$) and the geometry of the feed channel ($d_{F,h}$, $\varepsilon_F$ and $H_F$) were obtained from regression of the pressure drop data through the feed channel of the 1.8″ × 12″ SWMM-1 module. In the SWMM-1

module, the maximum cut off (the ratio of the permeate flow rate to the feed flow rate) was lower than 3%. It was therefore assumed that the concentration and velocity in the feed channel were uniform. The final correlation for the overall feed pressure drop in the module therefore, can be described by Eqs. (28) and (29).

$$\Delta P_F^{module} = \frac{a_F}{2d_{F,h}}\left(\frac{\rho\left(x_F^{inlet}\right)u_F^{inlet}d_{F,h}}{\mu\left(x_F^{inlet}\right)}\right)^{b_F}\rho(u_F^{inlet})^2\,L_F \tag{28}$$

$$u_F^{inlet} = \frac{J_F^{inlet}\nu\left(x_F^{inlet}\right)}{(N_L \times H_F L_F \varepsilon_F)} \tag{29}$$

$x_F^{inlet}$, $u_F^{inlet}$ and $J_F^{inlet}$ are the solute molar fraction, the velocity and the molar flow rate in the feed inlet, respectively. The pressure drop of the module, $\Delta P_F^{module}$, was measured experimentally, as the difference between the pressure drop in the housing in the presence of the module, $\Delta P_F^{module+housing}$, and the pressure drop of the empty housing $\Delta P_F^{empty\ housing}$ (see Eq. (30)).

$$\Delta P_F^{module} = \Delta P_F^{module+housing} - \Delta P_F^{empty\ housing} \tag{30}$$

The unknown parameters ($a_F$, $b_F$, $d_{F,h}$, $\varepsilon_F$ and $H_F$) were obtained from regression of the 12 experimental pressure drop data through the feed channel of the $1.8'' \times 12''$ SWMM-1 module ($\Delta P_F^{module}$) using Eqs. (28) and (29) (see Fig. 3(b)).

The pressure drop through the permeate channel was also calculated using the friction coefficient correlation in the form of Eq. (1), and this equation was reformulated as Eq. (31), to describe the permeate pressure drop along the elemental volume.

$$P_P^{j+1} = P_P^j - \frac{a_P}{2d_{P,h}}\left(\frac{\rho\left(x_P^{i,j}\right)u_{i,j,P}d_{P,h}}{\mu\left(x_P^{i,j}\right)}\right)^{b_P}\rho u_{i,j,P}^2\,\Delta y^j \tag{31}$$

$a_P$ and $b_P$ are the coefficient and the exponent of the correlation for the friction coefficient in the permeate channel, represented by Eq. (1), respectively. $d_{P,h}$ is the hydraulic diameter in the permeate channel and $\Delta y^j$ is the length of the element $i \times j$ along $y$ axis. The pressure in the outlet of the permeate channel (close to the central permeate tube) was assumed to be the atmospheric pressure. The local velocity in the permeate channel ($u_{i,j,P}$) was calculated as Eq. (32).

$$u_{i,j,P} = \frac{2 \times J_P^{i,j}\nu\left(x_P^{i,j}\right)}{\Delta x^i H_P \varepsilon_P} \tag{32}$$

$H_P$ is the height of the permeate channel and $\varepsilon_P$ is the void fraction of the permeate channel. On the permeate side of the module, it is not possible to experimentally measure the pressure drop through the permeate channel, since three sides of the permeate channel are sealed by glue lines. Thus it is not possible to apply direct regression to obtain the parameters describing the coefficient and the exponent of the Reynolds number in the friction coefficient correlation for the permeate channel ($a_P$ and $b_P$), and the geometry of the permeate channel ($d_{P,h}$, $\varepsilon_P$ and $H_P$). Similarly, the coefficient and the exponents in the Sherwood number correlation for the feed channel ($\alpha$, $\beta$ and $\lambda$), represented by Eqs. (33) and (34), cannot be obtained by performing direct regression of the mass transfer coefficient data, since the mass transfer coefficient was not experimentally measured. Here the contribution of the permeate flux on the mass transfer in the film is ignored, in agreement with Schock and Miquel [9], since the permeation velocities are orders of magnitude smaller compared to the convective crossflow velocities in the feed channels.

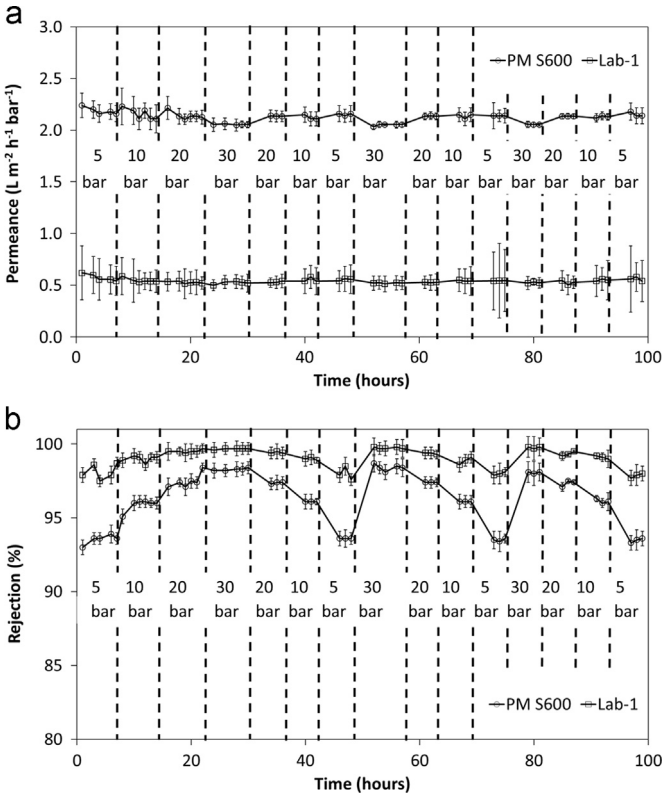



**Fig. 5.** Performance of flat sheet PuraMem® S600 and Lab-1 membranes tested in 1 g $L^{-1}$ SoA in EA solution at 30 °C and various pressures over time. (a) Permeance; (b) rejection of SoA.

**Table 3**
Membrane transport model parameters for PuraMem® S600 and Lab-1 membranes: $P_{m,1}$ is the solute permeability coefficient and $P_{m,2}$ is the solvent permeability coefficient.

| | PuraMem® S600 | Lab-1 |
|---|---|---|
| $P_{m,1}$ (mol $m^{-2}$ $s^{-1}$) | 2.06E−3 | 1.66E−4 |
| $P_{m,2}$ (mol $m^{-2}$ $s^{-1}$) | 1.59 | 0.40 |

$$Sh = \frac{k_F^{i,j}d_{F,h}}{D_{(x_R^{i,j})}} = \alpha Re^{\beta}Sc^{\lambda} = \alpha\left(\frac{d_{F,h}\rho_{(x_R^{i,j})}u_{i,j,F}}{\mu_{(x_R^{i,j})}}\right)^{\beta}\left(\frac{\mu_{(x_R^{i,j})}}{\rho_{(x_R^{i,j})}D_{(x_R^{i,j})}}\right)^{\lambda} \tag{33}$$

$$u_{i,j,F} = \frac{\sum_{j=1}^{n} J_R^{i,j}\nu\left(x_R^{i,j}\right)}{N_L \times H_F L_F \varepsilon_F} \tag{34}$$

$u_{i,j,F}$ is the local velocity in the feed channel. All 8 unknown parameters ($a_P$, $b_P$, $d_{P,h}$, $\varepsilon_P$, $H_P$, $\alpha$, $\beta$ and $\lambda$) were therefore determined together by performing indirect regression of the experimental flux and rejection data through the SWMM-1 module (in total, 36 flux data and 27 rejection data were available) using the combination of the film theory and the classical solution diffusion model, considering the gradients of concentrations, pressures and velocities (see Fig. 3(b)). The pre-determined classical solution-diffusion permeability coefficients, the friction coefficient correlation in the feed channel and the parameters describing the geometry of the feed channel were used in this step.

All regressions were performed in the MATLAB environment, using the built-in function *lsqcurvefit*. The regression implements a local search mechanism (i.e. gradient search) to obtain solutions that optimise the associated criterion function. The function uses a

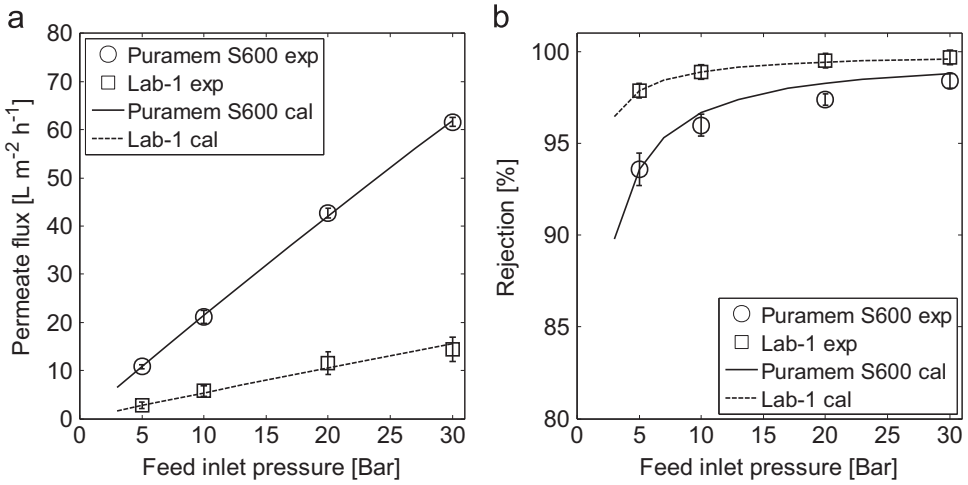



**Fig. 6.** Experimental and calculated performance of flat sheet PuraMem® S600 and Lab-1 membranes tested in 1 g $L^{-1}$ SoA in EA solution at 30 °C and various pressures. (a) Permeate flux; (b) rejection of SoA.

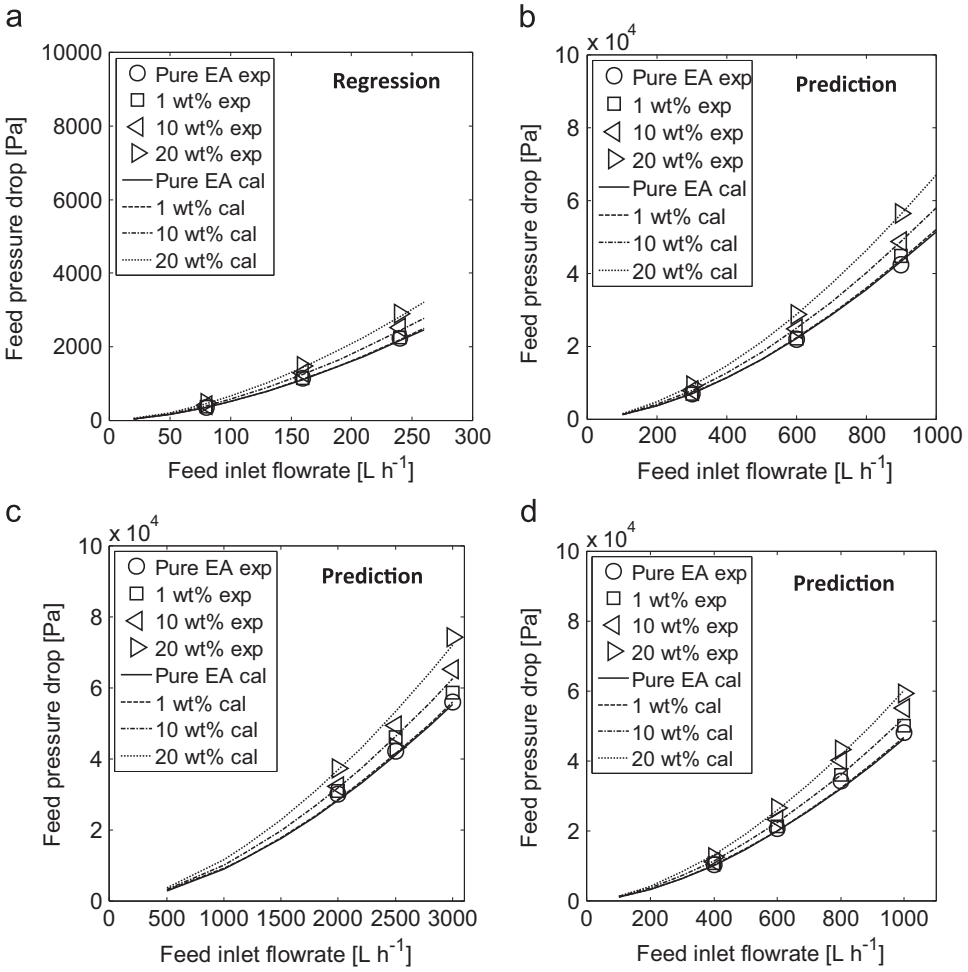



**Fig. 7.** Experimental and calculated pressure drop through the feed channel of different modules: (a) 1.8″ × 12″ SWMM-1; (b) 2.5″ × 40″ SWMM-2; (c) 4.0″ × 40″ SWMM-3; (d) 2.5″ × 40″ SWMM-4. Data from (a) only were used in the regression procedure.

"trust-region-reflective" algorithm, which requires a determined or overdetermined system of equations. It means that the number of independent equations must be at least equal to the number of fitting parameters. In this work, an overdetermined system was applied to perform all regressions, to minimise the effect of possible experimental outliers.

*3.2.3. Prediction of performance for spiral-wound membrane modules of different size and fabricating using different types of membranes*

The SWMM-2 and SWMM-3 modules were fabricated with the same type of feed and permeate spacers and with the same membranes as the SWMM-1 module, but with larger sizes (2.5″ × 12″ and 4.0″ × 40″, respectively). In the 4.0″ × 40″ SWMM-3

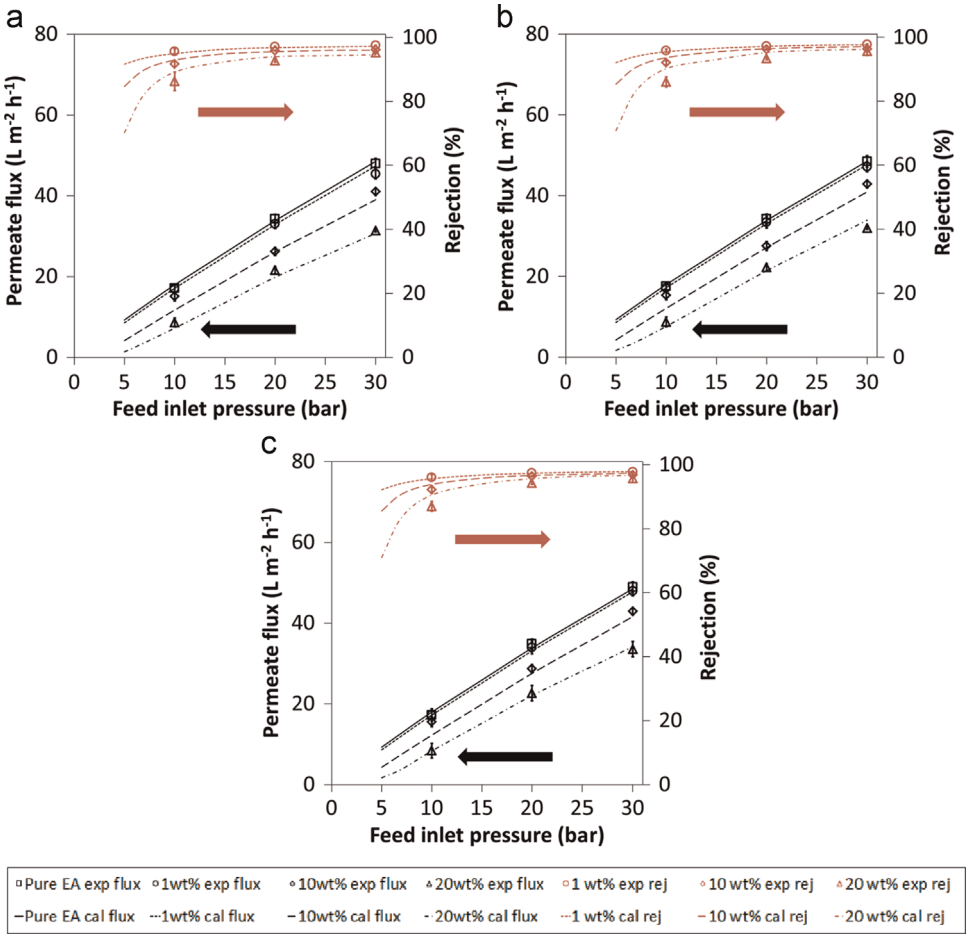



**Fig. 8.** Experimental and calculated flux (black) and rejection (red) of the 1.8″ × 12″ SWMM-1 module tested in 0–20 wt% SoA in EA solutions at 30 °C and various pressures (10, 20 and 30 bar) with different retentate flowrates: (a) 80 L $h^{-1}$; (b) 160 L $h^{-1}$; (c) 240 L $h^{-1}$. The performance of the 1.8″ × 12″ SWMM-1 module was used to perform regression to obtain the correlations for characterising pressure drops and mass transfer as well as the parameters describing both feed and permeate spacers. (For interpretation of the references to colour in this figure legend, the reader is referred to the web version of this article.)

module test, the solute concentration of the feed solution at the inlet of the module ($C_{1,F}$) was different from the concentration of the starting solution in the feed tank ($C_{1,FT}$), due to the two-pump configuration system (see Fig. 2(c)). The concentration of the feed solution at the inlet of the module ($C_{1,F}$) was calculated according to a mass balance on both inner and outer loops (see Eq. (35)).

$$C_{1,F} = \frac{(F'_R + F_P)C_{1,FT}}{F_R + F_P} + \frac{(F_R - F'_R)}{F_R + F_P}\frac{(F_P + F'_R)C_{1,FT} - F_P C_{1,P}}{F'_R} \quad (35)$$

$F_R$ and $F'_R$ are the retentate flowrates through the module and after the back pressure valve, respectively (see Fig. 2(c)). $F_P$ is the permeate flowrate. Since the system under study is a highly rejected system ($C_p \approx 0$), Eq. (35) was simplified as Eq. (36):

$$C_{1,F} = \frac{(F'_R + F_P)C_{1,FT}}{F_R + F_P} + \frac{(F_R - F'_R)}{F_R + F_P}\frac{(F_P + F'_R)C_{1,FT}}{F'_R} \quad (36)$$

It is assumed that the geometry of the channels is the same for modules made of the same spacers but different sizes and/or membranes. The performance of the SWMM-2 and SWMM-3 modules was then predicted using the combination of the film theory and the classical solution diffusion model, considering the gradients of pressures, concentrations and velocities, based on the pre-determined membrane transport model parameters; the semi-empirical correlations for the friction coefficient in both the feed and permeate channels; the semi-empirical correlation for the mass transfer coefficient in the feed channel and the pre-determined parameters describing the geometry of the feed and permeate channels (see Fig. 3(c)).

On the other hand, the 2.5″ × 40″ SWMM-4 module was fabricated with a different type of membrane (Lab-1) but with the same feed and permeate spacers as the other 3 modules. The membrane permeability coefficients for the Lab-1 membrane were again obtained by performing regression of experimental data for the flat sheet Lab-1 membrane (flux and rejection) using Eqs. (18) and (19). Afterwards, the same prediction procedure as for the SWMM-2 and SWMM-3 modules was performed (see Fig. 3(c)).

## 4. Results and discussion

### 4.1. Effects of time and pressure on membrane performance

OSN polymeric membranes can compact over time and pressure, as a consequence of their more or less open structure and crosslinking degree [25]. In order to understand the transport through the membranes in this study, it is important to check whether any irreversible compaction occurs over pressure and time. Fig. 5 shows the performance of both PM S600 and Lab-1 flat sheet membranes, tested in 1 g $L^{-1}$ SoA in EA solution, over time and at different pressure values. In Fig. 5, the bars represent the deviation of the experimental data among the 8 cells. The permeance through both membranes is almost independent of the

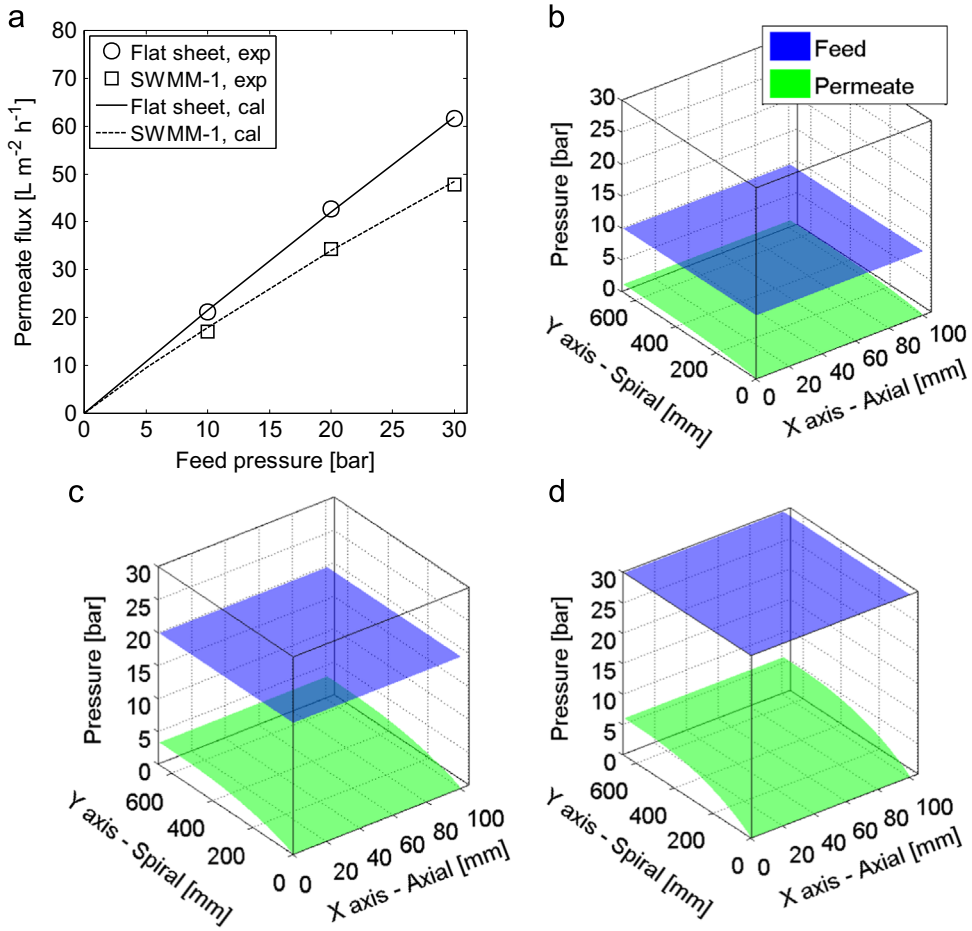



**Fig. 9.** Permeate flux and pressure profiles through the SWMM-1 module tested in pure EA at 30 °C and different pressures, with a retentate flowrate of 80 L $h^{-1}$. (a) Experimental and calculated permeate flux through flat sheet PM S600 membranes and the SMWW-1 module. (b) pressure profile in both feed and permeate channels in the SWMM-1 module at the initial feed pressure of 10 bar; (c) pressure profile in both feed and permeate channels in the SWMM-1 module at the initial feed pressure of 20 bar; (d) pressure profile in both feed and permeate channels in the SWMM-1 module at the initial feed pressure of 30 bar.

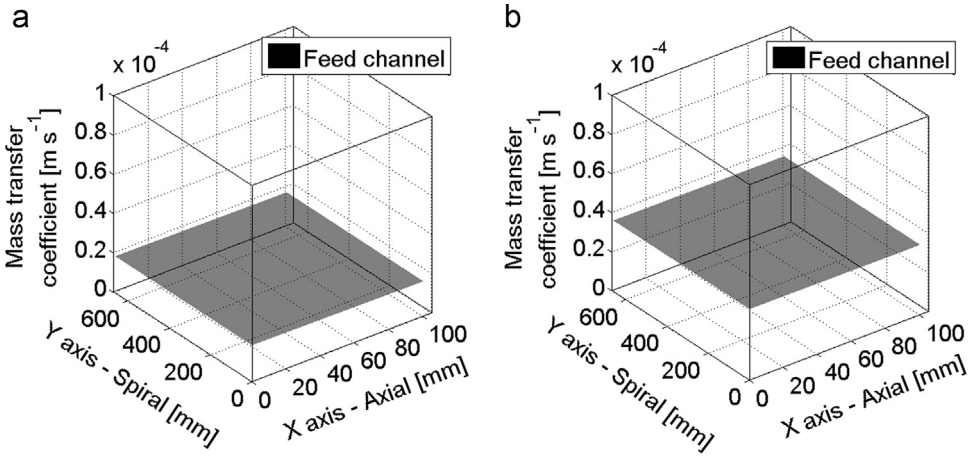



**Fig. 10.** Profiles of mass transfer coefficient in the feed channel of the SWMM-1 module in 1 wt% SoA in EA solution at 30 bar with different retentate flowrates: (a) 80 L $h^{-1}$; (b) 240 L $h^{-1}$.

pressure (see Fig. 5(a)), while the rejection is positively affected by the pressure: the higher the pressure, the higher the rejection (see Fig. 5(b)). Moreover, the membrane performance (in terms of both flux and rejection) of both membranes showed negligible change after the membranes were compressed at high pressure, indicating that these membranes do not undergo any significant irreversible compaction.

### *4.2. Regression of flat sheet membrane data to obtain the permeability coefficient*

The membrane transport model parameters for both PM S600 and Lab-1 membranes were determined by regressing the performance of flat sheet data at 5 bar, using the classical solution diffusion model, represented by Eqs. (18) and (19). According to this model, the model parameters to be determined are the solute

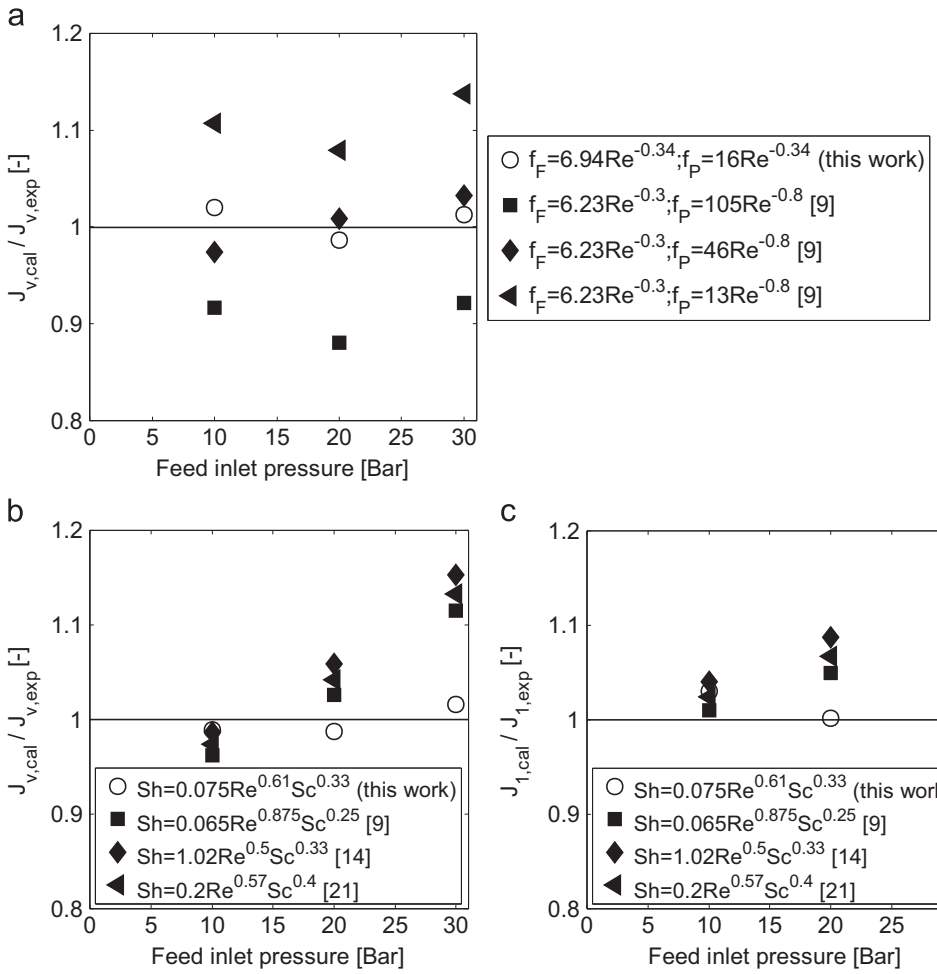



**Fig. 11.** Calculated total volumetric flux and SoA molar flux in the SWMM-1 module, normalised with respect to the experimental data. (a) Calculated total volumetric flux in the SWMM-1 module in pure EA at 30 °C and various pressures with a retentate flowrate of 80 L h$^{-1}$ using different friction coefficient correlations from this work and Schock and Miquel [9]; (b, c) Calculated total volumetric flux (b) and SoA molar flux (c) in the SWMM-1 module in 20 wt% solution at 30 °C and various pressures with a retentate flowrate of 240 L h$^{-1}$ using the friction coefficient correlations from this work and different mass transfer correlations from this work and Schock and Miquel [9], Schwinge et al. [14], Koutsou et al. [21].

and solvent permeability coefficients, respectively. The regressed values of these parameters are reported in Table 3.

These transport parameters were then used to predict the performance of the same flat sheet membranes at different pressure values, from 5 to 30 bar. Good agreement between calculated and experimental flux and rejection was observed, as shown in Fig. 6(a) and (b), respectively. In Fig. 6, the bars represented the deviation of the experimental data among the 8 cells. The values of *resnorm* for PM S600 and Lab-1 membranes are 9.1E−03 and 4.2E−02, respectively. These very small values confirmed that the classical solution diffusion model is suitable to describe the membrane transport through these two types of membranes at different pressures.

### 4.3. Regression of SWMM-1 module performance to obtain the correlations for pressure drop and mass transfer coefficient in the feed channel and the spacer geometry

The coefficient and the exponents in the friction coefficient correlation for the feed channel ($a_F$ and $b_F$) and the parameters describing the feed channel geometry ($d_{F,h}$, $\varepsilon_F$ and $H_F$) were determined by regressing the feed pressure drop data in the SWMM-1 module, using Eqs. (27) and (28). The correlation for the friction coefficient in the feed channel thus obtained is represented as Eq. (37).

$$f_F = a_F\, Re^{b_F} = a_F\left(\frac{d_{F,h}\rho_F\, u_F}{\mu_F}\right)^{b_F} = 6.94Re^{-0.34} \tag{37}$$

The values of the parameters describing the hydraulic diameter ($d_{F,h}$), void fraction ($\varepsilon_F$) and height of the feed channel ($H_F$) are 0.79 mm, 0.827 and 0.77 mm, respectively. Good agreement between the calculated and the experimental pressure drop data for the SWWM-1 module, characterised by a *resnorm* of 3.1E−02, is shown in Fig. 7(a). Furthermore, good prediction of the feed pressure drop in the other three modules is also shown in Fig. 7(b), (c) and (d). The *resnorm* values in the SWMM-2, SWMM-3 and SWMM-4 modules were 1.0E−02, 8.7E−02 and 5.6E−02, respectively. This proves that the friction coefficient correlation for the feed channel and the parameters describing the geometry of the feed channel, obtained from the regression of the SWWM-1 module performance data, successfully describe the pressure drop in the channels filled with the same feed spacer.

It is worth noting that the feed pressure drop through all the modules is low (<1 bar). Although the feed pressure drop is negligible for our simulation, we decided to include it in the modelling procedure anyway, to keep our modelling framework as generic as possible. In fact, feed pressure drops may be more significant in other industrial configurations, such as arrays of

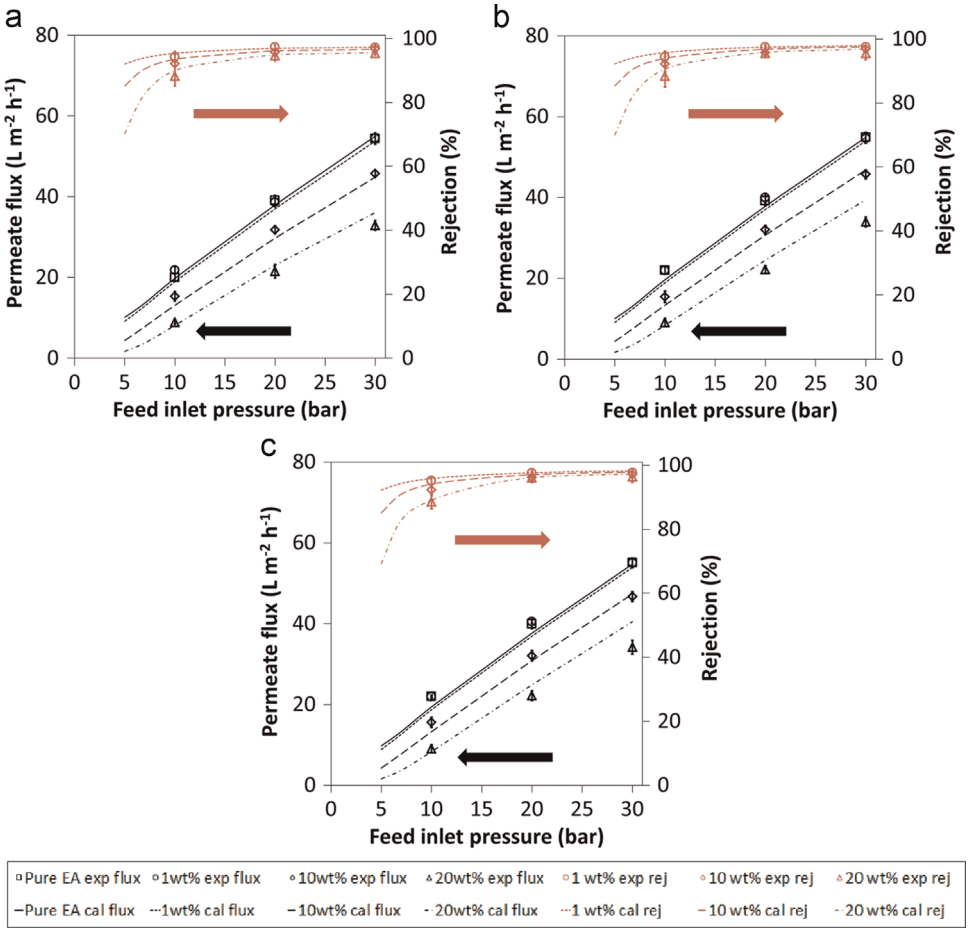



**Fig. 12.** Experimental and calculated flux (black) and rejection (red) of the 2.5″ × 40″ SWMM-2 module tested in 0–20 wt% SoA in EA solutions at 30 °C and various pressures (10, 20 and 30 bar) with different retentate flowrates: (a) 300 L h$^{-1}$; (b) 600 L h$^{-1}$; (c) 900 L h$^{-1}$. The performance of the 2.5″ × 40″ SWMM-2 module was not used in the regression procedure, but only used to validate the predictive capability of the correlations developed in this work. (For interpretation of the references to colour in this figure legend, the reader is referred to the web version of this article.)

several spiral-wound membrane modules connected in series [8,24].

The coefficient and the exponent of the Reynolds number in the friction coefficient correlation for the permeate channel ($a_P$ and $b_P$), the parameters describing the permeate channel ($d_{P,h}$, $\varepsilon_P$ and $H_P$) and the coefficient and the exponents in the Sherwood number correlation ($\alpha$, $\beta$ and $\lambda$) were determined by performing regression of the SWMM-1 module performance (flux and rejection), using the combination of the film theory and the classical solution diffusion model, considering gradients of pressures, concentrations and velocities. The regression was made use of the permeability coefficients, the friction coefficient correlation for the feed channel and the parameters describing the feed channel obtained from previous regression procedures. It is important to note that, in this step, both fluid dynamics and mass transfer characteristics were regressed at the same time. The friction coefficient correlation for the permeate channel is described by Eq. (38) and the Sherwood number correlation for the feed channel is described by Eq. (39), respectively.

$$f_P = a_P\, Re^{b_P} = a_P\left(\frac{d_{P,h}\rho_P\, u_P}{\mu_P}\right)^{b_P} = 16Re^{-0.34} \tag{38}$$

$$Sh = \alpha\, Re^{\beta}\, Sc^{\lambda} = 0.075\, Re^{0.61}\, Sc^{0.33} \tag{39}$$

The values of the hydraulic diameter ($d_{P,h}$), void fraction ($\varepsilon_P$) and height of the permeate channel ($H_P$) are 0.048 mm, 0.315 and 0.27 mm, respectively. Good agreement between experimental and calculated membrane module performance, characterised by a *resnorm* value of 6.1E−02, is shown in Fig. 8, in terms of both membrane flux and rejection.

When comparing the permeance of the SWMM-1 module fabricated with the PM S600 membrane with the flat sheet PM S600 membrane in pure EA, it is noticeable that the permeate flux through the SWMM-1 module is lower (see Fig. 9(a)): specifically, the higher the feed pressure, the bigger the difference between module flux and flat sheet membrane flux. The main reason for this divergence is the presence of the pressure drop in the permeate channel, which causes a reduction in the effective differential pressure between the retentate and permeate channels in the module with increasing feed pressure. The extent of the pressure in both the feed and permeate channels in the SWMM-1 module, at different operating pressures (10–30 bar), is shown in Fig. 9(b), (c) and (d). Clearly, at 30 bar, the pressure drop is more significant than at 10 bar (see Figs. 9(d) and (b)).

As shown in Fig. 10, the mass transfer coefficient in the SWMM-1 module had an order of magnitude of $10^{-5}$ m s$^{-1}$. Although gradients of velocity and concentration were present along the module, the mass transfer coefficient was found to be almost constant along the feed channel.

Finally, the correlations found in this work, for both friction coefficient and mass transfer coefficient, were compared with similar correlations from the literature [9,14,21]. These correlations were used to predict flux and SoA rejection in the SWMM-1

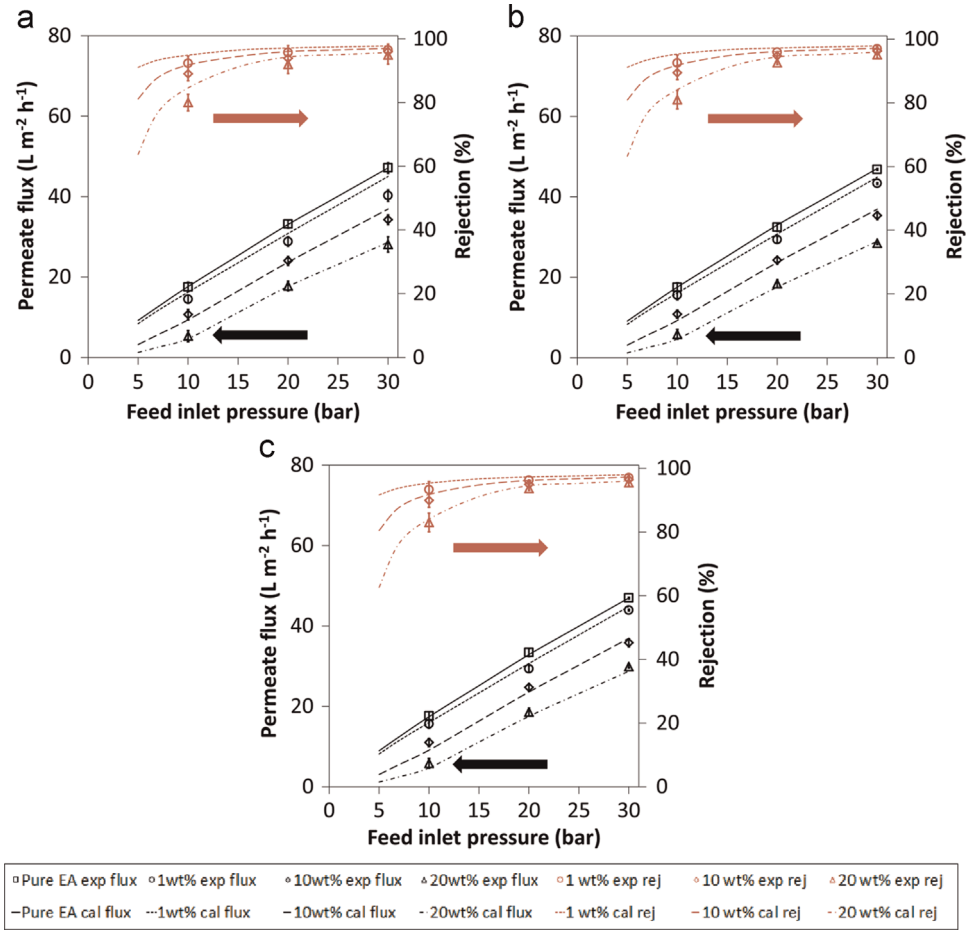



**Fig. 13.** Experimental and calculated flux (black) and rejection (red) of the 4.0″ × 40″ SWMM-3 module tested in 0–20 wt% SoA in EA solutions at 30 °C and various pressures (10, 20 and 30 bar) with different retentate flowrates: (a) 2000 L $h^{-1}$; (b) 2500 L $h^{-1}$; (c) 3000 L $h^{-1}$. The performance of the 4.0″ × 40″ SWMM-3 module was not used in the regression procedure, but only used to validate the predictive capability of the correlations developed in this work. (For interpretation of the references to colour in this figure legend, the reader is referred to the web version of this article.)

module. Fig. 11 clearly shows that the correlations from references [9,14,21], mainly obtained from indirect measurements and CFD simulations in aqueous solutions, were not suitable to describe the performance of the SWMM-1 module in all operating conditions, while the correlations developed in this work provided the best match with the experimental data. The biggest improvement of the correlations developed in this work, with respect to the ones from literature, was found in the description of the solvent flux in pure EA (see Fig. 11(a)) and in the description of the total volumetric flux and the solute molar flux under high pressure conditions in highly concentrated solution (see Fig. 11(b) and (c)). One possible reason for the difference is that the valid range of the Reynolds and Schmidt numbers in the correlations adopted from the literature is not exact the same as the range in this work. Specifically in Fig. 11(a), the Reynolds number in the feed channel was about 45 and it was between 5 and 19 in the permeate channel. The correlations adopted from Schock and Miquel [9] for the friction coefficients in both feed and permeate channels were validated in the Reynolds number range of 50–1000 and 20–100, respectively. In Fig. 11(b) and (c), the Reynolds and Schmidt numbers in the feed channel were about 250 and 440, respectively, and the correlations adopted from the literature were validated in different ranges: [9] for $150 < Re < 400$, $Sc = 660$; [14] for $90 < Re < 700$, $Sc = 2.09E5$; [21] for $50 < Re < 200$, $1450 < Sc < 5550$. It is also worth to mention that the range of Reynolds and Schmidt numbers is wide in OSN due to the variety of solutes and solvents, and very likely the correlations derived from aqueous solutions cannot cover the ranges of Reynolds and Schmidt numbers for OSN applications.

### 4.4. Prediction of spiral wound membrane module performance

Figs 12–14 show both experimental and predicted fluxes and rejections in all the modules not used in the regression procedure, under various operating conditions. It is clear that both fluxes and rejections decreased when the concentration of the solution increased, due to the occurrence of osmotic pressures and concentration polarisation. Furthermore, the figures show that both the fluxes and rejections increased with the feed pressure. More importantly, good agreement between the experimental and predicted data, characterised by the small values of *resnorm* (6.9E−02, 6.1E−02 and 9.1E−02 for the SWMM-2, SWMM-3 and SWMM-4 modules, respectively), was observed in all cases.

Fig. 15 shows that the mass transfer coefficient in these three modules (SWMM-2, SWMM-3 and SWMM-4) has an order of magnitude of $10^{-5}$ m $s^{-1}$, similar to the SWMM-1 module (see Fig. 10). Although these modules have longer feed channels with respect to the SWMM-1 module, the mass transfer coefficients did not change significantly along the feed channel.

Finally, these results show that the empirical correlations determined from the regression of the smallest module (SWWM-1, 1.8″ × 12″) can be extended to describe the fluid dynamics and mass transfer characteristics in other modules, which have larger sizes and/or are made of a different membrane material. They

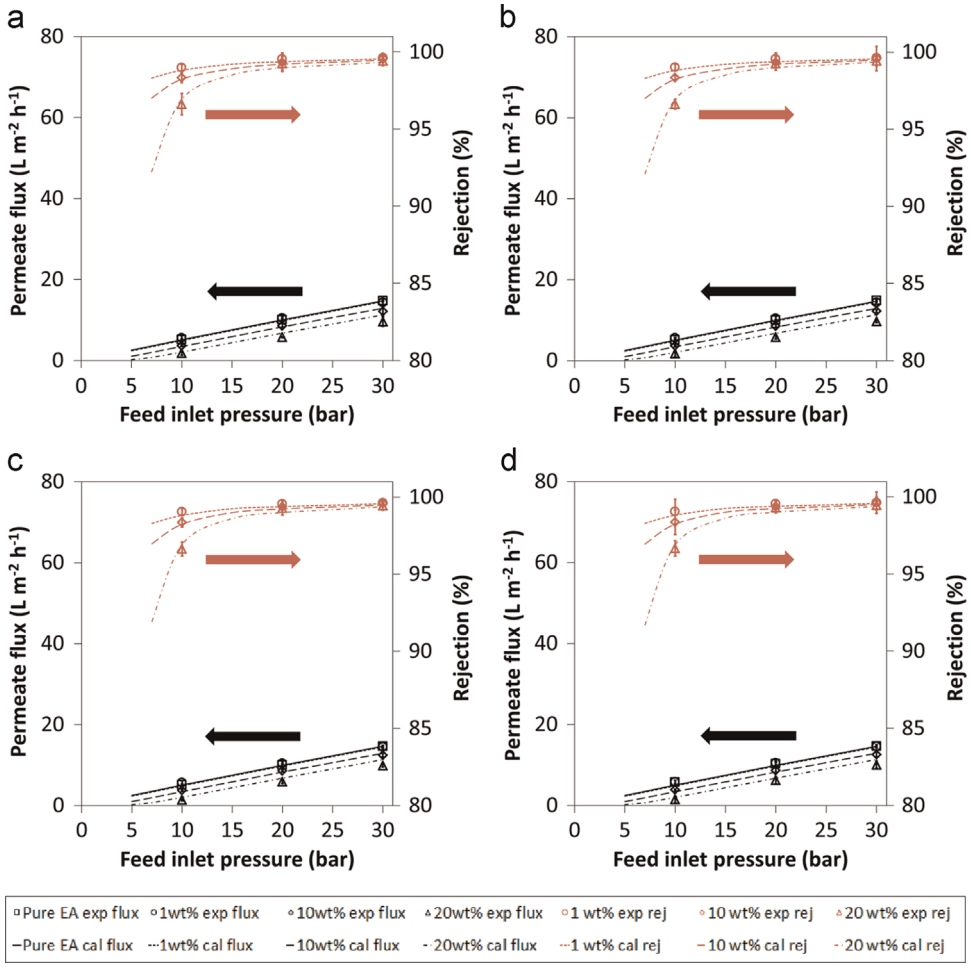



**Fig. 14.** Experimental and calculated flux (black) and rejection (red) of the 2.5″ × 40″ SWMM-4 module tested in 0–20 wt% SoA in EA solutions at 30 °C and various pressures (10, 20 and 30 bar) with different retentate flowrates: (a) 400 L $h^{-1}$; (b) 600 L $h^{-1}$; (c) 800 L $h^{-1}$; (d) 1000 L $h^{-1}$. The performance of the 2.5″ × 40″ SWMM-4 module was not used in the regression procedure, but only used to validate the predictive capability of the correlations developed in this work. (For interpretation of the references to colour in this figure legend, the reader is referred to the web version of this article.)

further show that the performance of a spiral-wound membrane module can be predicted from simple flat sheet laboratory measurements, as long as the fluid dynamics and mass transfer characteristics in the spiral-wound membrane module are known. In this work, the Reynolds number in the feed channel was between 45 and 600; the Schmidt number in the feed channel was between 200 and 440; and the Reynolds number in the permeate channel was lower than 22. We believe that the correlations obtained in this work could be used to describe the fluid dynamics and mass transfer characteristics in any spiral-wound membrane module which is made of the same feed and permeate spacers, and used in the applications where Reynolds and Schmidt numbers are in a similar range, as mentioned above.

## 5. Conclusions

This paper reports the performance of four spiral-wound membrane modules tested in 0–20 wt% solutions of sucrose octaacetate in ethyl acetate under various pressures and retentate flowrates. These modules were made of two different types of membranes (a commercial membrane, PuraMem® S600, and a development product, Lab-1, from Evonik MET) and covered three module sizes (1.8″ × 12″, 2.5″ × 40″ and 4.0″ × 40″). All modules had the same feed and permeate spacers (referred to as EMET-F3 and EMET-P1, respectively). Initially the effects of time and pressure on flat sheet membrane were investigated. The permeance through both membranes was almost independent of the pressure, while the rejection was positively affected by the pressure: the higher the pressure, the higher the rejection. Moreover, the membrane performance (in terms of both flux and rejection) showed negligible change after the membrane was compressed at high pressure, indicating that these membranes did not undergo any significant irreversible compaction.

The classical solution–diffusion model was selected to describe the transport through the membrane. The unknown model parameters were determined from regression of experimental flat sheet data at one unique pressure value. These parameters were then used to predict the performance of the flat sheet membranes under different pressures and good agreement was observed for both types of membranes (PM S600 and Lab-1). This indicated that the classical solution diffusion model was adequate to describe the transport through the membranes in this study. A correlation to characterise the friction coefficient in the feed channel was determined by regression of the feed pressure drop data through the 1.8″ × 12″ (SWWM-1) module. During the same regression procedure, the parameters describing the feed channel, necessary to calculate the Reynolds number, were also obtained. These fitting parameters were then used to predict the feed pressure drops in the other three modules and good agreement was observed between calculated and experimental data. A similar correlation for the friction coefficient in the permeate channel and a correlation

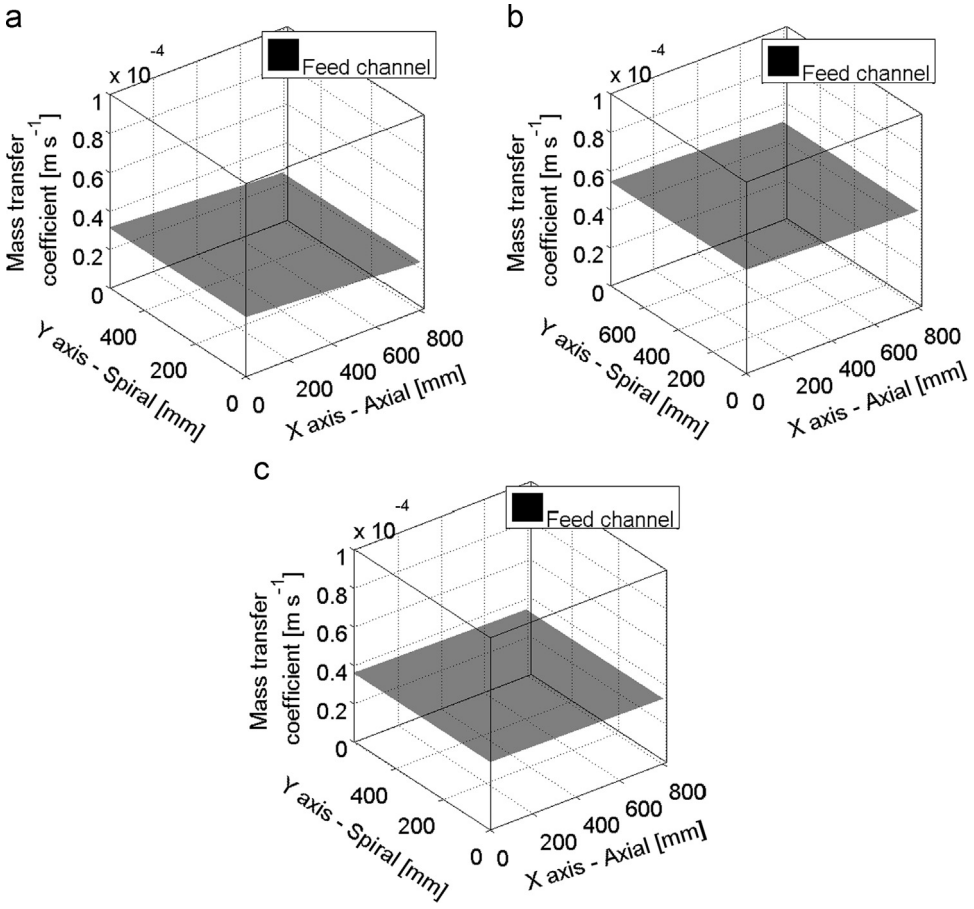



**Fig. 15.** Profiles of mass transfer coefficients in the feed channel of the different modules in 1 wt% SoA in EA solution at 30 bar and 30 °C with different retentate flowrates. (a) SWMM-2 module with a retentate flowrate of 300 L $h^{-1}$; (b) SWMM-3 module with a retentate flowrate of 2000 L $h^{-1}$; (c) SWMM-4 module with a retentate flowrate of 400 L $h^{-1}$.

for the mass transfer coefficient in the feed channel were determined by regression of the $1.8'' \times 12''$ performance data (in terms of both flux and rejection). Here the classical solution diffusion model combined with the film theory was used, with the consideration of the gradients of concentration, pressure, velocity and mass transfer coefficient through the module. The parameters describing the permeate channel were also obtained in the same regression procedure.

The three empirical correlations thus obtained, for the friction coefficients in the feed and permeate channels and the mass transfer coefficient in the feed channel, respectively, were used to predict the performance of all other modules used in this study. Good agreement was observed, which proves that the empirical correlations determined from the regression of the smallest module ($1.8'' \times 12''$) can be extended to describe the fluid dynamics and mass transfer characteristics in other modules, which have larger sizes and/or are made of different membranes. We believe that the correlations obtained in this work could be used to describe the fluid dynamics and mass transfer characteristics in any spiral-wound membrane module which is fabricated using the same feed and permeate spacers, and used in the applications where (i) Reynolds number in feed channel is in the range between 45 and 600; (ii) Schmidt number in feed channel is between 200 and 440; and (iii) Reynolds number in permeate channel is lower than 22.

**Acknowledgements**

The research leading to these results had received funding from the European Community's Seventh Framework Programme under grant agreement MemTide 238291 FP7-PEOPLE-ITN-2008 and from EPSRC under the Project EP/J014974/1 entitled Molecular Builders: Constructing Nanoporous Materials.

**Nomenclature**

*List of symbols*

| | |
|---|---|
| $A$ | effective membrane area ($m^2$) |
| $a$ | coefficient in friction coefficient correlation (dimensionless) |
| $b$ | exponent of Reynolds number in friction coefficient correlation (dimensionless) |
| $C_i$ | concentration of species $i$ (mol $m^{-3}$) |
| $D$ | diffusivity of solute in solvent ($m^2$ $s^{-1}$) |
| $d_h$ | hydraulic diameter (m) |
| $F$ | feed volumetric flowrate ($m^3$ $s^{-1}$) |
| $f$ | friction coefficient (dimensionless) |
| $F'_R$ | retentate flowrate after back pressure valve ($m^3$ $s^{-1}$) |
| $H$ | height of channel (m) |
| $J$ | molar flowrate (mol $s^{-1}$) |
| $J_i$ | molar permeate flux of species $i$ (mol $m^{-2}$ $s^{-1}$) |

| | |
|---|---|
| $J_y$ | volumetric permeate flux ($m^3\ m^{-2}\ s^{-1}$) |
| $\tilde{J}$ | local permeate molar flowrate through element ($mol\ s^{-1}$) |
| $k$ | mass transfer coefficient ($m\ s^{-1}$) |
| $L$ | length of channel (m) |
| $N_L$ | number of membrane leaves (dimensionless) |
| $P$ | pressure (Pa) |
| $P_{m,i}$ | permeability coefficient of species $i$ ($mol\ m^{-2}\ s^{-1}$) |
| $R$ | ideal gas constant ($Pa\ m^3\ mol^{-1}\ K^{-1}$) |
| $Re$ | Reynolds number (dimensionless) |
| $Rej_i^{obs}$ | observed rejection of species $i$ (%) |
| $Sc$ | Schmidt number (dimensionless) |
| $Sh$ | Sherwood number (dimensionless) |
| $resnorm$ | the norm of residuals (dimensionless) |
| $T$ | temperature (K) |
| $t$ | permeation time (s) |
| $u$ | linear velocity of flow ($m\ s^{-1}$) |
| $\bar{u}$ | average linear velocity of flow ($m\ s^{-1}$) |
| $V$ | permeate volumetric flowrate ($m^3\ s^{-1}$) |
| $W$ | width of the channel (m) |
| $x_i$ | molar fraction of species $i$ in solution (dimensionless) |
| $\tilde{x}$ | local solute molar fraction in solution through element (dimensionless) |
| $\bar{x}$ | average solute molar fraction (dimensionless) |
| $\Delta P$ | Pressure drop (Pa) |
| $\Delta x^i$ | length of element $i \times j$ along $x$ axis (m) |
| $\Delta y^j$ | length of element $i \times j$ along $y$ axis (m) |

*Greek symbols*

| | |
|---|---|
| $\alpha$ | coefficient in Sherwood number correlation (dimensionless) |
| $\beta$ | exponent of Reynolds number in Sherwood number correlation (dimensionless) |
| $\lambda$ | exponent of Schmidt number in Sherwood number correlation (dimensionless) |
| $\rho$ | density ($kg\ m^{-3}$) |
| $\mu$ | dynamic viscosity ($kg\ m^{-1}\ s^{-1}$) |
| $\nu_i$ | molar volume of species $i$ ($m^3\ mol^{-1}$) |
| $\varepsilon$ | void fraction (dimensionless) |
| $\gamma_i$ | activity coefficient of species $i$ (dimensionless) |

*Subscripts*

| | |
|---|---|
| 1 | solute |
| 2 | solvent |
| *ave* | average |
| *exp* | experimental |
| *F* | feed solution or feed channel |
| *FM* | feed side membrane–liquid interface |
| *P* | permeate solution or permeate channel |
| *R* | retentate |

*Superscripts*

| | |
|---|---|
| $i$ | position $i$ in the direction of $x$ axis |
| $j$ | position $j$ in the direction of $y$ axis |

## References


[1] P. Marchetti, M.F. Jimenez Solomon, G. Szekely, A.G. Livingston, Molecular separation with organic solvent nanofiltration: a critical review, Chem. Rev. 114 (2014) 10735.

[2] G. Szekely, M.F. Jimenez Solomon, P. Marchetti, J.F. Kim, A.G. Livingston, Sustainability assessment of organic solvent nanofiltration: from fabrication to application, Green Chem. 16 (2014) 4440.

[3] I. Sereewatthanawut, F.W. Lim, Y.S. Bhole, D. Ormerod, A. Horvath, A.T. Boam, A.G. Livingston, Demonstration of molecular purification in polar aprotic solvents by organic solvent nanofiltration, Org. Process Res. Dev. 14 (2010) 600.

[4] S. Darvishmanesh, L. Firoozpour, J. Vanneste, P. Luis, J. Degrève, B.V. der Bruggen, Performance of solvent resistant nanofiltration membranes for purification of residual solvent in the pharmaceutical industry: experiments and simulation, Green Chem. 13 (2011) 3476.

[5] D. Peshev, A.G. Livingston, OSN Designer, a tool for predicting organic solvent nanofiltration technology performance using Aspen One, MATLAB and CAPE OPEN, Chem. Eng. Sci. 104 (2013) 975.

[6] D. Peshev, L.G. Peeva, I.I.R. Baptista, A.T. Boam, Application of organic solvent nanofiltration for concentration of antioxidant extracts of rosemary (Rosmarinus officiallis L.), Chem. Eng. Res. Des. 89 (2011) 318.

[7] J. Vanneste, D. Ormerod, G. Theys, D.V. Gool, B.V. Camp, S. Darvishmanesh, B. V. der Bruggen, Towards high resolution membrane based pharmaceutical separations, J. Chem. Technol. Biotechnol. 88 (2013) 98.

[8] P. Silva, L.G. Peeva, A.G. Livingston, Organic solvent nanofiltration (OSN) with spiral-wound membrane elements – highly rejected solute system, J. Membr. Sci. 349 (2010) 167.

[9] G. Schock, A. Miquel, Mass transfer and pressure loss in spiral wound modules, Desalination 64 (1987) 339.

[10] A.R. Johnson, Experimental investigation of polarization effects in reverse osmosis, J. AIChE 20 (1974) 996.

[11] J. Balster, I. Punt, D.F. Stamatialis, M. Wessling, Multi-layer spacer geometries with improved mass transport, J. Membr. Sci. 282 (2006) 351.

[12] O. Kuroda, S. Takahashi, M. Nomura, Characterisation of flow and mass transfer rate in an electrodialyzer compartment including spacer, Desalination 46 (1983) 225.

[13] A.R. Da Costa, A.G. Fane, C.J.D. Fell, A.C.M. Franken, Optimal channel spacer design for ultrafiltration, J. Membr. Sci. 62 (1991) 275.

[14] J. Schwinge, D.E. Wiley, A.G. Fane, R. Guenther, Characterization of a zigzag spacer for ultrafiltration, J. Membr. Sci. 172 (2000) 19.

[15] A.R. Da Costa, A.G. Fane, D.E. Wiley, Spacer characterization and pressure drop modelling in spacer-filled channels for ultrafiltration, J. Membr. Sci. 87 (1994) 79.

[16] S.K. Karode, A. Kumar, Flow visualization through spacer filled channels by computational fluid mechanics. I. Pressure drop and shear stress calculations for flat sheet geometry, J. Membr. Sci. 193 (2001) 69.

[17] F. Li, W. Meindersma, A.B. de Haan, T. Reith, Optimization of commercial net spacers in spiral would membrane modules, J. Membr. Sci. 208 (2002) 289.

[18] F. Li, G.W. Meindersma, A.B. de Haan, T. Reith, Optimization of non-woven spacers by CFD and validation by experiments, Desalination 146 (2002) 209.

[19] F. Li, W. Meindersma, A.B. de Haan, T. Reith, Experimental validation of CFD mass transfer simulations in flat channels with non-woven net spacers, J. Membr. Sci. 232 (2004) 19.

[20] G.A. Fimbres-Weihs, D.E. Wiley, Numerical study of mass transfer in three-dimensional spacer-filled narrow channels with steady flow, J. Membr. Sci. 306 (2007) 228.

[21] C.P. Koutsou, S.G. Yiantsios, A.J. Karabelas, A numerical and experimental study of mass transfer in spacer-filled channels: effects of spacer geometrical characteristics and Schmidt number, J. Membr. Sci. 326 (2009) 234.

[22] M. Kostoglou, A.J. Karabelas, Comprehensive simulation of flat-sheet membrane element performance in steady state desalination, Desalination 316 (2013) 91.

[23] A.J. Karabelas, C.P. Koutsou, M. Kostoglou, The effect of spiral would membrane element design characteristics on its performance in steady state desalination – a parametric study, Desalination 332 (2014) 76.

[24] J. Schwinge, P.R. Neal, D.E. Wiley, D.F. Fletcher, A.G. Fane, Spiral wound modules and spacers review and analysis, J. Membr. Sci. 242 (2004) 129.

[25] P. Marchetti, A.G. Livingston, Predictive membrane transport models for organic solvent nanofiltration: how complex do we need to be? J. Membr. Sci. 476 (2015) 530.

[26] S.J. Han, S.S. Luthra, L.G. Peeva, X.J. Yang, A.G. Livingston, Insights into the transport of toluene and phenol through organic solvent nanofiltration membranes, Sep. Sci. Technol. 38 (9) (2003) 1899.

[27] L.G. Peeva, E. Gibbins, S.S. Luthra, L.S. White, R.P. Stateva, A.G. Livingston, Effect of concentration polarisation and osmotic pressure on flux in organic solvent nanofiltration, J. Membr. Sci. 236 (2004) 121.